The fusion crust of the Winchcombe meteorite: A preserved record of atmospheric entry processes

Matthew J. Genge, Luke Alesbrook, Natasha V. Almeida, Helena C. Bates, Phil A. Bland, Mark R. Boyd, Mark J. Burchell, Gareth S. Collins, Luke T. Cornwell, Luke Daly, et al.

The Meteoritical Society

Meteoritics & Planetary Science 1–25 (2023)
doi: 10.1111/maps.13937

The fusion crust of the Winchcombe meteorite: A preserved record of atmospheric entry processes

Matthew J. GENGE[1,2]*, Luke ALESBROOK[3], Natasha V. ALMEIDA[2], Helena C. BATES[2], Phil A. BLAND[4], Mark R. BOYD[1], Mark J. BURCHELL[3], Gareth S. COLLINS[1], Luke T. CORNWELL[3], Luke DALY[5,6,7], Hadrien A. R. DEVILLEPOIX[4], Matthias van GINNEKEN[3], Ansgar GRESHAKE[8], Daniel HALLATT[3,9], Christopher HAMANN[8], Lutz HECHT[8,10], Laura E. JENKINS[5], Diane JOHNSON[11], Rosie JONES[12], Ashley J. KING[2], Haithem MANSOUR[12], Sarah MCMULLAN[1], Jennifer T. MITCHELL[13], Gavyn ROLLINSON[14], Sara S. RUSSELL[2], Christian SCHRÖDER[15], Natasha R. STEPHEN[13], Martin D. SUTTLE[16], Jon D. TANDY[17], Patrick TRIMBY[12], Eleanor K. SANSOM[4], Vassilia SPATHIS[3], Francesca M. WILLCOCKS[13], and Penelope J. WOZNIAKIEWICZ[3]

[1]Department of Earth Science and Engineering, Imperial College London, London SW7 2A, UK
[2]Planetary Materials Group, Natural History Museum, London SW7 5BD, UK
[3]Department of Physics and Astronomy, Centre for Astrophysics and Planetary Science, University of Kent, Canterbury, Kent CT2 7NH, UK
[4]Space Science and Technology Centre (SSTC), School of Earth and Planetary Science, Curtin University, Perth, Western Australia 6102, Australia
[5]School of Geographical and Earth Sciences, University of Glasgow, Glasgow G12 8QQ, UK
[6]Australian Centre for Microscopy and Microanalysis, The University of Sydney, Camperdown, New South Wales 2006, Australia
[7]Department of Materials, University of Oxford, Oxford OX1 3PH, UK
[8]Museum für Naturkunde, Leibniz-Institut für Evolutions- und Biodiversitätsforschung, Invalidenstr. 43, 10115 Berlin, Germany
[9]University of Lille, CNRS, INRAE, Centrale Lille, UMR 8207 – UMET Unité Materiaux et Transformations, F-59000 Lille, France
[10]Institut für Geologische Wissenschaften, Freie Universität Berlin, Malteserstraße 74-100, Berlin 12249, Germany
[11]School of Aerospace, Transport and Manufacturing, Cranfield University, Cranfield, Bedfordshire MK43 0AL, UK
[12]Oxford Instruments Nanoanalysis, Halifax Road, High Wycombe HP12 3SE, UK
[13]Plymouth Electron Microscopy Centre, University of Plymouth, Devon PL4 8AA, UK
[14]Camborne School of Mines, University of Exeter, Penryn Campus, Penryn TR10 9FE, UK
[15]Biological and Environmental Sciences, University of Stirling, Stirling FK9 4LA, UK
[16]Faculty of Science, Technology, Engineering and Mathematics, The Open University, Walton Hall, Milton Keynes MK7 6AA, UK
[17]Department of Chemistry and Forensic Science, Centre for Astrophysics and Planetary Science, University of Kent, Canterbury CT2 7NZ, UK
*Corresponding author. E-mail: m.genge@imperial.ac.uk

(Received 03 June 2022; revision accepted 24 October 2022)

Abstract–Fusion crusts form during the atmospheric entry heating of meteorites and preserve a record of the conditions that occurred during deceleration in the atmosphere. The fusion crust of the Winchcombe meteorite closely resembles that of other stony meteorites, and in particular CM2 chondrites, since it is dominated by olivine phenocrysts set in a glassy mesostasis with magnetite, and is highly vesicular. Dehydration cracks are unusually abundant in Winchcombe. Failure of this weak layer is an additional ablation mechanism to produce large numbers of particles during deceleration, consistent with the observation of pulses of plasma in videos of the Winchcombe fireball. Calving events might provide an observable phenomenon related to meteorites that are particularly susceptible to

dehydration. Oscillatory zoning is observed within olivine phenocrysts in the fusion crust, in contrast to other meteorites, perhaps owing to temperature fluctuations resulting from calving events. Magnetite monolayers are found in the crust, and have also not been previously reported, and form discontinuous strata. These features grade into magnetite rims formed on the external surface of the crust and suggest the trapping of surface magnetite by collapse of melt. Magnetite monolayers may be a feature of meteorites that undergo significant degassing. Silicate warts with dendritic textures were observed and are suggested to be droplets ablated from another stone in the shower. They, therefore, represent the first evidence for intershower transfer of ablation materials and are consistent with the other evidence in the Winchcombe meteorite for unusually intense gas loss and ablation, despite its low entry velocity.

INTRODUCTION

Fusion crust is the thermally altered outer layer of a meteorite and forms owing to heating during deceleration in the atmosphere (e.g., Ramsdohr, 1967). Often fusion crust is avoided and ignored in studies of meteorites because in this region, the primary mineralogical and chemical properties of the meteorite are changed by heating. Fusion crust does, however, provide insights into the process occurring during atmospheric entry, which owing to their dependence on entry angle and velocity, may relate to orbital parameters, and thus have genetic significance (Genge & Grady, 1999a; Krinov, 1960). Furthermore, while meteorites often fragment into hundreds, or even thousands of individual stones, a much larger number of ablation debris particles are likely to have been produced by the removal of surface melt during flight and are difficult to distinguish from micrometeorites (Badyukov et al., 2011; Badyukov & Raitala, 2012). Indeed, observations of smoke trails reported for some meteorite falls, and not others, indicate varying production of ablation debris and recondensed smokes (Miller et al., 2013). These particles are likely to be distributed over larger areas than meteorites, and in those meteoroids that completely evaporate, may provide the only lasting record of the fall (Artemieva & Shuvalov, 2016; Badyukov et al., 2011; Badyukov & Raitala, 2012). Interpreting observations of fusion crusts in terms of the physical and chemical behavior of meteorites during atmospheric flight, however, are complicated by incomplete data on the atmospheric phenomena that occurred during falls and the absence of entry parameters in most cases.

The CM2 Winchcombe meteorite fell at 9:54 p.m. on February 28, 2021 in Gloucestershire in the United Kingdom and was recovered over the next week as described in King et al. (2022). Critically, the meteorite fireball was observed by the meteoroid camera networks in the United Kingdom (UKFAll; Daly et al., 2020); UKFN/GFO (Devillepoix et al., 2020); UKMON (Campbell-Burns & Kacerek, 2014); NEMETODE (Stewart et al., 2013); SCAMP/FRIPON (Colas et al., 2012); GMN (Vida et al., 2021); AllSky7 (Hankey et al., 2020) providing an accurate orbit and a predicted fall ellipse (McMullan et al., 2022). Furthermore, the fireball was recorded on security and dashcam videos, owing to its fall over a densely populated area, providing a record of the visible phenomena occurring during the event. The Winchcombe meteorite thus provides an opportunity to investigate how the mineralogical, textural, and compositional properties of meteorite fusion crusts might be related to the behavior of specific meteoroids during atmospheric deceleration, and perhaps even their atmospheric entry parameters.

Previous studies of fusion crust show they comprise of an outer melted crust and an inner thermally altered substrate (Genge & Grady, 1999a; Ramsdohr, 1967). The outer melted crust has experienced a high degree of partial melting, but usually contains some high-temperature relict phases, such as forsteritic olivine, enstatite, and chromite. Most of the melted crust is dominated by quench phases and/or glass. Vesicles and immiscible metal and sulfide droplets also occur in the outer melted crust. In contrast, the thermally altered substrate has experienced much lower degrees of partial melting, which decreases with distance into the meteorite. Melting and remobilization of eutectic Fe-S liquids (Ramsdohr, 1967) and of glass within chondrule mesostasis occurs in the thermally altered substrate, particularly close to the outer melted crust (Genge & Grady, 1999a). Thermal decomposition of temperature-sensitive mineral phases also occurs within the thermally altered substrate with breakdown of phyllosilicates into dehydroxylates, and the dissociation or organic matter and carbonates (Court & Sephton, 2009; Genge & Grady, 1999a).

The compositions of meteorite fusion crusts have been shown to be closely similar to the bulk composition of the meteorite, but have experienced loss of volatile elements, such as S (e.g., Genge & Grady, 1999a). Further chemical modification of fusion crust relative to bulk meteorite relates to local variations owing to incomplete diffusion under highly nonequilibrium melting conditions and magma mixing owing to the extrusion of melts from

the thermally altered substrate into the outer melted fusion crust.

While the majority of outer melted crusts are dominated by olivine phenocrysts, magnetite and wustite crystals, and glass, textures vary with meteorite group and between stones of the same shower, depending on their exact thermal history during deceleration (Genge & Grady, 1999a). Variations in fusion crusts also occur owing to oxidation by atmospheric gas, with increasing oxidation outward depending on the oxidation state of the host meteorite (Genge & Grady, 1999b; Pittarello et al., 2019).

In this paper, the mineralogy, texture, and composition of the fusion crust of the Winchcombe meteorite are described, providing the first analysis of a meteorite with a known orbit and well-observed fall phenomena. Several previously unknown processes, such as thermal pulsing by calving events, explosive outgassing, transfer of interstone spray, and fusion crust expansion and collapse, are suggested by the petrology of the crust. The results also allow the nature of meteoroid ablation debris to be inferred.

SAMPLES AND METHODS

Observations were made on several stones of the Winchcombe fall, including hand specimen and as resin-mounted polished blocks. Polished blocks P30551 (sample 5a-v1-4; BM.2022,M9-13), P30555 (sample 5a-v1-7; BM.2022,M9-17), P30554 (Sample 5a-v1-6; BM.2022,M9-16), P30542 (sample 1b-43; BM.2022,M2-44), and P30540 (sample 1b-v1-4; BM.2022,M2-42) were studied by analytical scanning electron microscope (SEM) with textural properties determined from backscattered electron images. Samples, including masses and collection information, are listed by King et al. (2022). Energy-dispersive spectroscopy (EDS) was used to determine phase compositions with X-ray mapping used to collect phase and compositional maps. Several different instruments were used to collect data: (1) Zeiss EVO at the Natural History Museum; (2) Hitachi TM4000+ at Imperial College London; (3) Hitachi S3400N, with an Oxford Instruments X-Max EDS SDD (with AZtex analysis software) at the University of Kent; (4) Zeiss Sigma variable pressure field emission gun SEM equipped with an X-Max 80 mm^2 silicon drift EDS detector from Oxford Instruments Nanoanalysis in the ISACC facility at the University of Glasgow; (5) Hitachi SU70 Schottky field emission gun SEM with EBSD Detector: Oxford Instruments Symmetry S2. Chemical analyses collected at 20 kV accelerating voltage, at a range of beam currents, depending on instrument, against gain calibrations made on cobalt and against internal standards. Matrix corrections were applied. Analytical uncertainties are typical of those of EDS techniques with minor elements (0.5 wt%) having ~50% uncertainties, while detection limits are on the order of 0.1–0.2 wt%. Mineral compositions reported in the paper all have compositions within 95% of ideal mineral stoichiometry—including analytical totals. Analyses of areas were performed using a rastered beam in order to provide approximate bulk compositions for fusion crust. Areas with large relict crystals and sulfides were avoided during these analyses.

Samples for electron backscatter detection (EBSD), performed at Oxford Instruments, were further prepared by vibratory polishing for 2 h 40 min with colloidal silica suspension, then coating with 5–10 nm of carbon. Analyses were carried out at 20 kV, 8.1 nA beam current and EBSD patterns were collected at 156 × 128 pixel resolution, typically at ~165 patterns per second. Indexing was carried out using forsterite olivine and magnetite spinel phases. Minor postacquisition data cleaning was used to remove isolated errors and to improve data at grain boundaries.

A Bruker M4 TORNADO PLUS micro X-ray fluorescence (μXRF) spectrometer at the Museum für Naturkunde, Berlin, was used to obtain major and trace element (>10 μg g^{-1}) abundances from polished block P30542 (sample 1b-43). An X-ray intensity overview map of 1147 width and 757 pixel height was obtained with a dwell time of 10 ms per pixel and under a vacuum of 2 mbar by using a rhodium X-ray source operated at 50 kV and 600 μA. The X-ray beam was focused to a spot of 20 μm diameter on the sample surface by using a polycapillary lens. Due to the fine-grained nature of the CM2 matrix and the small dimensions of sample P30542, the overview map was slightly oversampled (5 μm pixel size) to allow the discrimination of fine details. The bulk composition of sample P30542 was determined from (1) a sum spectrum of 224,800 pixels obtained from the pristine, interior part of the sample; and (2) a grid of 113 randomly placed, 20 μm spot analyses that were obtained using 50 kV, 300 μA, and 300 s integration time per spot. Care was taken in both approaches to exclude the fusion crust, the thermally altered substrate, and substrate close to the outer, presumably thin parts of the sample. Standardization of the μXRF data was based on a custom type calibration routinely in use for this instrument and data quality was checked against a slab of the Murchison CM2 carbonaceous chondrite.

RESULTS

Macroscopic Observations

In hand specimen, stones of Winchcombe vary from those covered by near-complete fusion crust to those with only small irregular islands of crust preserved. The fusion crust varies in luster from submetallic to dull in luster, with a color from gray to slightly copper-colored (submetallic areas). The fusion crust is a lighter color

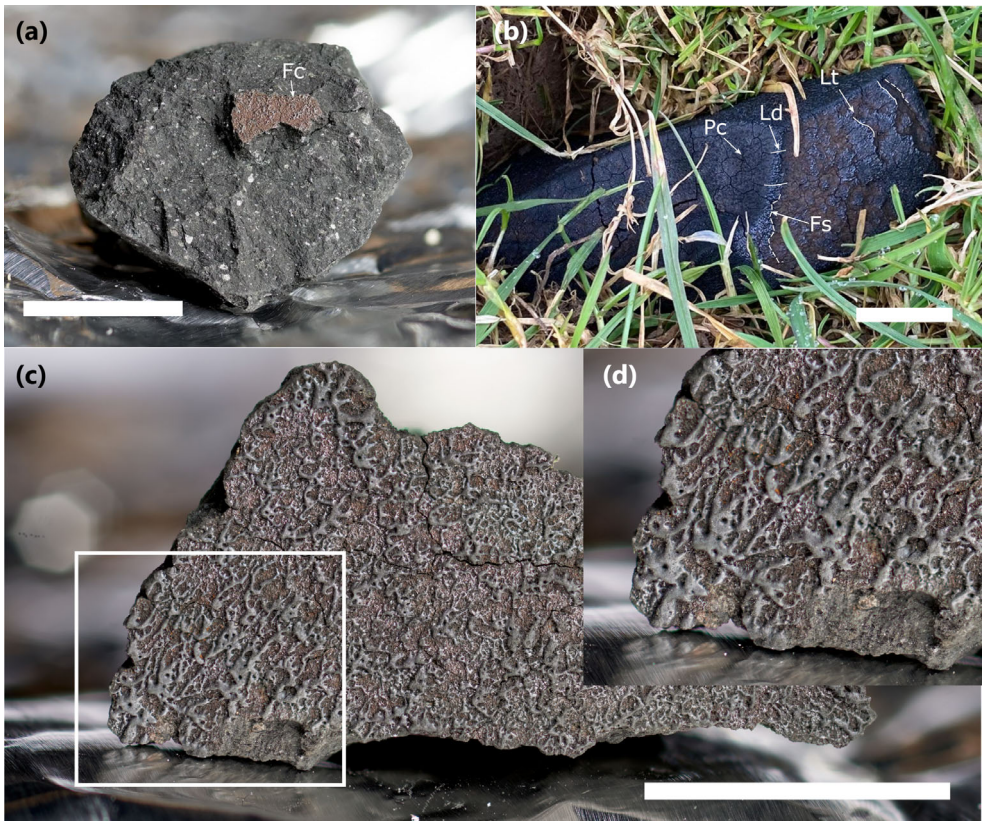

Fig. 1. External morphology of the fusion crust on Winchcombe. a) Delamination of fusion crust (fc). b) Polygonal cracks (pc), longitudinal flow ridges (lc), lateral flow ridges (lt), and fracture surfaces (fs) on the surface of a stone. c) Fusion crust on a flat face showing flow ridges and areas with minimal melted crust development. d) A magnified area of image (c). Scale bars are 1 cm in size.

than the matrix in the interior of the stone. A full description of the petrology of the interior is given in Suttle et al. (this volume), Daly et al. (this volume), and King et al. (2022).

The small-scale features on the fusion crust differ between stones. The fusion crust is usually covered by small (sub-mm) fractures with a broadly polyhedral shape. Surface protrusions occur at a sub-mm scale. On some faces, these are arcuate features with no preferred orientation (Fig. 1a and 1c), while on other faces, there are longitudinal sublinear ridges with a preferred orientation and lateral ridges with cuspate morphologies. Longitudinal ridges appear superimposed on lateral ridges (Fig. 1b). Some faces also show fracture surfaces where thickness of the melted crust abruptly decreases (Fig. 1b). Submillimeter vesicles varying from subspherical to irregular smooth cavities are common.

Microscopic Observations

Structure of Fusion Crust

The structure of fusion crust on Winchcombe varies between specimens, in particular in the depth of the outer melted and thermally altered crust, although this variation is at least in part the result of the plane of section in polished blocks (Fig. 2). The outer melted crust is identified on the basis of its igneous textures, comprising euhedral crystals within glass. This crust contains >3 vol% relict, unmelted phases, identified by their irregular shapes and Mg-rich compositions (forsterite $<Fa_4$ and enstatite $<Fs_4$). The thermally altered substrate in contrast is identified by the near absence of euhedral crystals, excluding pre-existing phases within chondrules, and the presence of fractures that extend into the meteorite.

Fractures are abundant in the thermally altered substrate, representing up to 5 vol% of the outer part of this layer, but become less abundant inward (Fig. 2a–c). These structures are frequently interconnecting and some surround isolated areas of thermally altered matrix, at least in the plane of section. Block P30551 samples only the thermally altered substrate and has a plane of section broadly parallel to the outer melted crust. In this specimen, the fractures have near polygonal intersection geometries (Fig. 2d). The distribution of fracture-bound matrix fragments is shown in Fig. 3 and has number density that increases with decreasing size. There are few

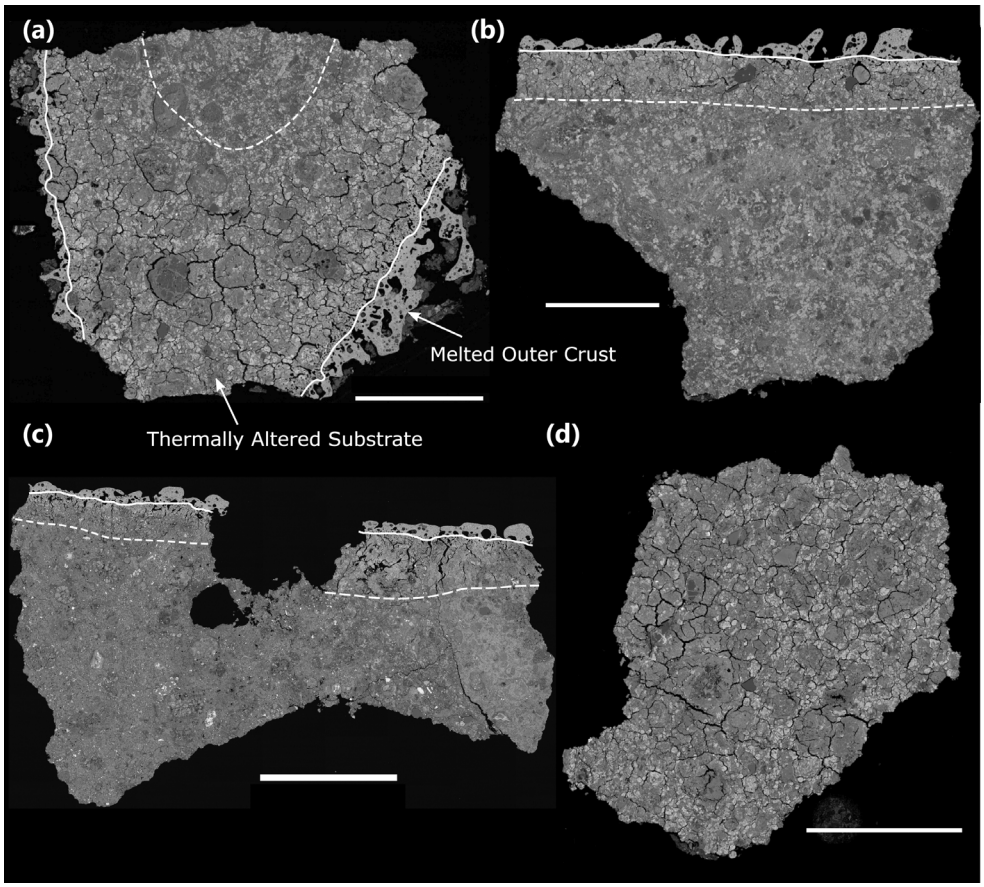

Fig. 2. Whole sample backscattered electron images of fusion crust. Solid white lines mark the boundary between the melted outer crust. Dashed lines show the approximate inner boundary of the thermally altered substrate, denoted by the disappearance of surface correlated fractures. a) Sample P30551. b) P30555. c) P30540. d) P30554, which comprises entirely of thermally altered substrate. Scale bars are 1 mm.

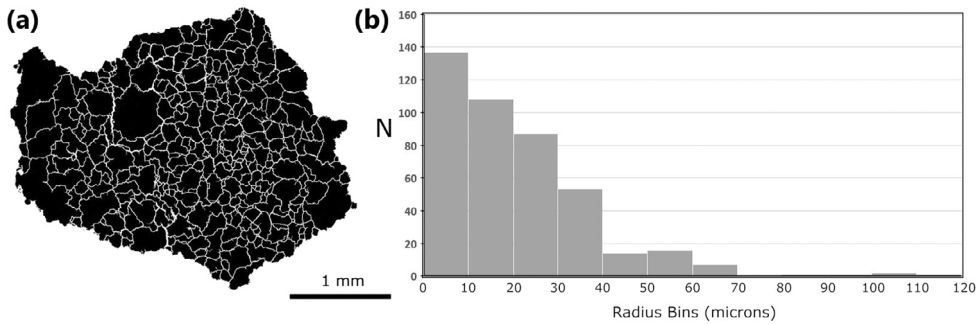

Fig. 3. Size distributions of areas encapsulated by fractures in the thermally altered substrate. Fractures were extended, at constant thickness, by 20% of their length to estimate how they might continue to develop during the fragmentation of the substrate (a). Areas of encapsulated areas were measured using ImageJ. b) The radii shown represent the dense rock equivalent radius of a circle of equal area, where density of the meteorite is taken as 2100 kg m^{-3} and the dense rock is 3000 kg m^{-3}.

fragments that have a radius of more than 70 μm. Radius here is expressed as the radius of a circle with an equivalent area, scaled from a density 2100–3000 kg m^{-3}. This calculation provides a radius representative of a liquid droplet formed by fusion of the fragments, assuming no significant mass loss by evaporation. Observations in sections cut broadly perpendicular to the melted crust indicate that fracture widths and abundances increase outward. The inner margin of the thermally altered substrate is defined in this paper by the disappearance of

surface-correlated fractures, below which no further textural or mineralogical evidence for atmospheric heating exists.

Some variation in fracture structure is observed depending on the lithology of the stone. The majority of stones comprise lithologies dominated by tochilinite inclusions (TCIs) within phyllosilicate (serpentine)-rich matrix with sparse, mostly pseudomorphed chondrules (B1/B2 CM2.1–2.4; King et al., 2022; Suttle et al., this volume). In contrast, one specimen (P30540) shows a change in the depth of the thermally altered from this material to lithology H (CM2.0), which has sparse TCIs (Fig. 2c).

The outer melted fusion crust has a thickness of up to 0.5 mm in the studied samples; however, it exhibits significant variations in thickness along its length (Fig. 2a–c). In places, cavities extend through the entire melted crust and expose the underlying thermally altered substrate. The surface topography of the crust, as seen in the plane of section, is irregular and has numerous lobe-shaped protrusions. Abundant vesicles are also present and generally increase in size, and decrease in abundance outward.

Texture and Mineralogy of the Thermally Altered Substrate

The texture of the thermally altered substrate varies with depth into the meteorite. At the innermost margin, as delimited by the termination of fractures, the texture and mineralogy are indistinguishable from the unaltered core of the meteorite (see Daly et al., this volume; King et al., 2022; Suttle et al., this volume). With decreasing depth, textural changes are first noted within tochilinite crystals within TCI and phyllosilicate clusters, with thin fractures observed following the median of tochilinite and small elongate cavities (<0.5 μm in length) appearing in the crystals (Fig. 4b and 4c). Outward toward the melted crust, the textures of TCI change continuously with increasing abundance of elongated smooth cavities and fractures within tochilinite crystals (Fig. 3e). Nickel-bearing sulfides (18–25 wt% Ni) occur and have sulphur contents suggesting they are pentlandite or troilite. In some areas they fill open fractures. The serpentine-rich areas of TCIs adopt increasingly homogeneous textures toward the melted crust with the disappearance of acicular to sheet-like crystal habits (Fig. 4d).

Thermal alteration within the matrix and within the mesostases of hydrous-altered chondrules is observed close to the melted crust (<0.5 mm). Textural changes are similar to those within the serpentine of TCI with a loss of acicular to sheet-like crystal morphologies on a submicron scale and the appearance of equant micron-scale silicate crystals with grain boundaries that have a diffuse appearance in backscattered electron intensity (Fig. 4e and 4g). Some areas with coarser sheet-like morphologies remain and typically have abundant cavities between sheet-like phases, particularly within the mesostases of aqueously altered chondrules (Fig. 4f).

Within ~0.2 mm of the melted outer crust, the matrix becomes increasingly homogeneous in texture, with sparse relict chromite, forsterite, and enstatite crystals within a vesicular groundmass. The groundmass contains equant subhedral crystals <0.3 μm in size and numerous submicron subspherical vesicles. Nickel-bearing sulfides (13–66 wt% Ni) occur as small (micron-scale) rounded grains, as veins filing fractures, or within areas with a network structure (Fig. 4g). The Ni content of the small grains is inferred from analyses assuming the surrounding silicate is nickel-free, and thus is likely to be an overestimate. The network structures have a textural resemblance to the structure of TCI in the deeper parts of the thermal substrate since they exhibit linear, bifurcating areas of sulfide of similar scale to tochilinite crystals, set in a groundmass of equant Fe-bearing silicates (Fig. 4g). Sulfide grains are particularly abundant in some areas immediately below the outer melted crust, comprising up to ~10 vol%.

Rounded, smooth cavities are abundant in the outer parts of the thermally altered substrate (30–70 vol%) and vary from <0.1 to 50 μm in size. Most large cavities are elongate and irregular. Some are highly elongate having apparent aspect ratios >10 and are thus similar to fractures. Nickel-bearing sulfide rims are observed partially coating cavities and lining some open fractures to the surface (Fig. 4h). In open fractures, magnetite with inclusions of Ni-bearing sulfide is present closer to the exterior of the meteorite.

Texture and Mineralogy of the Outer Melted Crust

The outer melted crust has a porphyritic texture and is highly vesicular. Grain size varies with depth, with submicron equant olivine crystals present at its base, adjacent to the thermally altered substrate, and olivine crystals up to 8 μm in diameter present at some locations close to the surface of the crust (Fig. 5). Magnetite crystals are also present and increase in size and abundance toward the exterior of the crust. Closest to the thermally altered substrate magnetite crystals are <0.1 μm in diameter, while near the surface, they reach 4 μm. Most are equant octahedra; however, some poorly developed cruciform habits also occur in some areas. Submicron regions within the cores of some magnetite crystals have higher backscattered potential and are interpreted as wüstite, but were not analyzed owing to their small size.

Olivine crystals are euhedral phenocrysts in the outer parts of the melted crust. In most areas, they have nearly homogeneous compositions (Fa_{18}) and are surrounded by

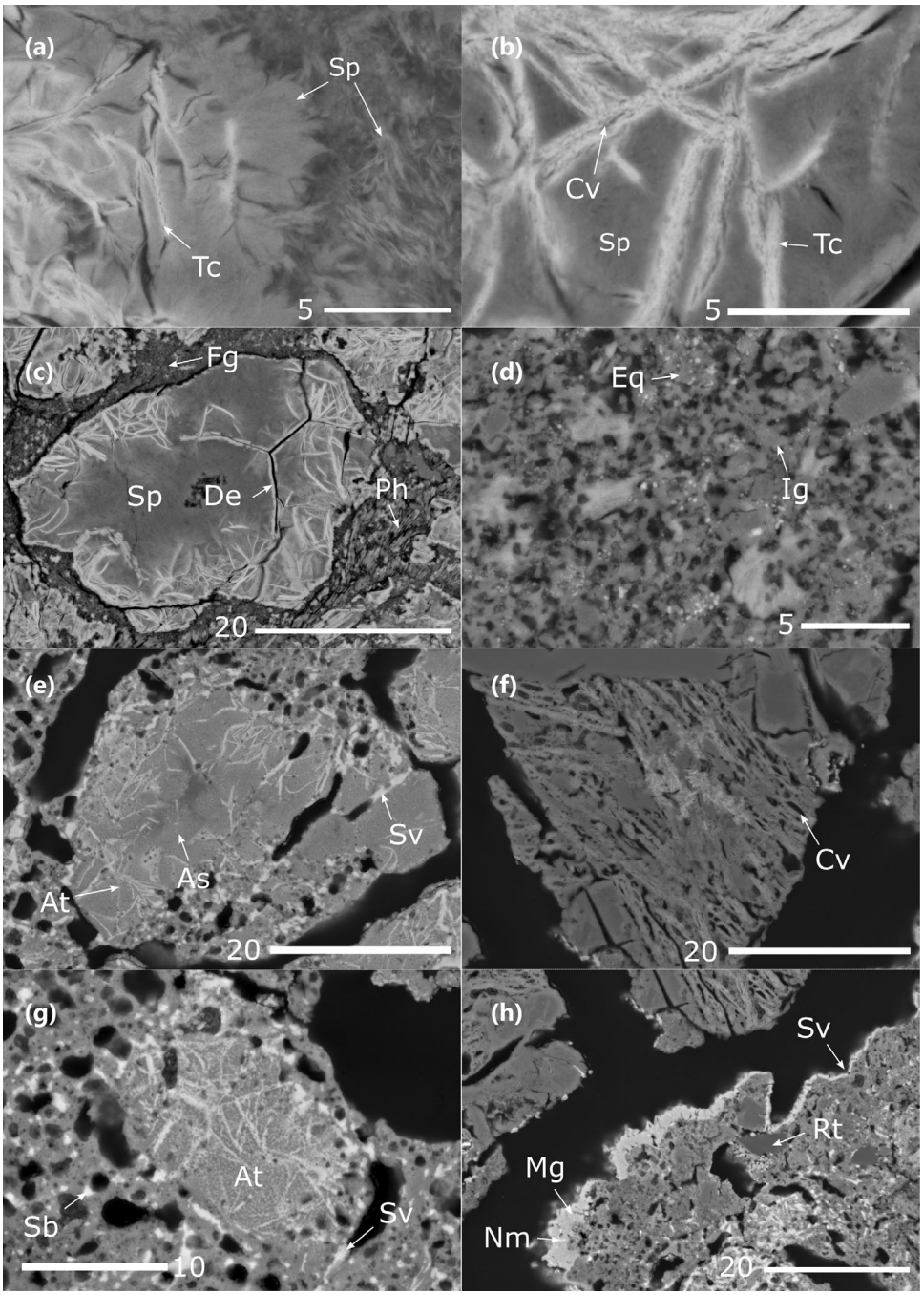

Fig. 4. Backscattered electron images of the thermally altered substrate (TAS). a) A tochilinite inclusion (TCI) in the deepest part of the TAS exhibiting serpentine (Sp) and tochilinite (Tc) with minor contraction cracks [P30551]. b) A TCI at 0.3 d (depth fraction of 0.3 into TAS). The tochilinite contains abundant small elongate cavities (Cv), while serpentine appears unaltered [P30551]. c) A TCI at dehydration cracks (De) following the center of tochilinite crystals [P30555]. Coarse (Ph) and fine (Fg) sheet-like phyllosilicates are present in the matrix. d) The matrix at 0.2 d in the TAS [P30551] contains abundant rounded cavities, irregular homogeneous amorphous silicates (Ig), and small equant crystalline phases. e) A TCI at 0.1 d in the TAS [P30551]. Altered tochilinite is present (At) and altered serpentine lacks crystallinity (As). Ni-bearing sulfides partly fill elongate cavities (Sv). f) Pseudomorphed chondrule mesostasis with abundant elongate cavities (Cv) [P30551]. g) An altered TCI (At) at 0.05d in TAS comprising elongate FeNiS after tochilinite and serpentine altered to submicron equant olivine [P30551]. The surrounding matrix is highly vesicular and contains abundant blebs of Ni-bearing sulfide (Sb). Some discontinuous veins of sulfide are present (Sv). h) A sulfide vein (Sv) coating an open fracture [P30551]. Sulfide is replaced by magnetite (Mg) containing inclusions of Ni-rich metal toward the exterior of the meteorite. The surrounding matrix contains some relict forsterite grains (Rt). All scales are in micrometer.

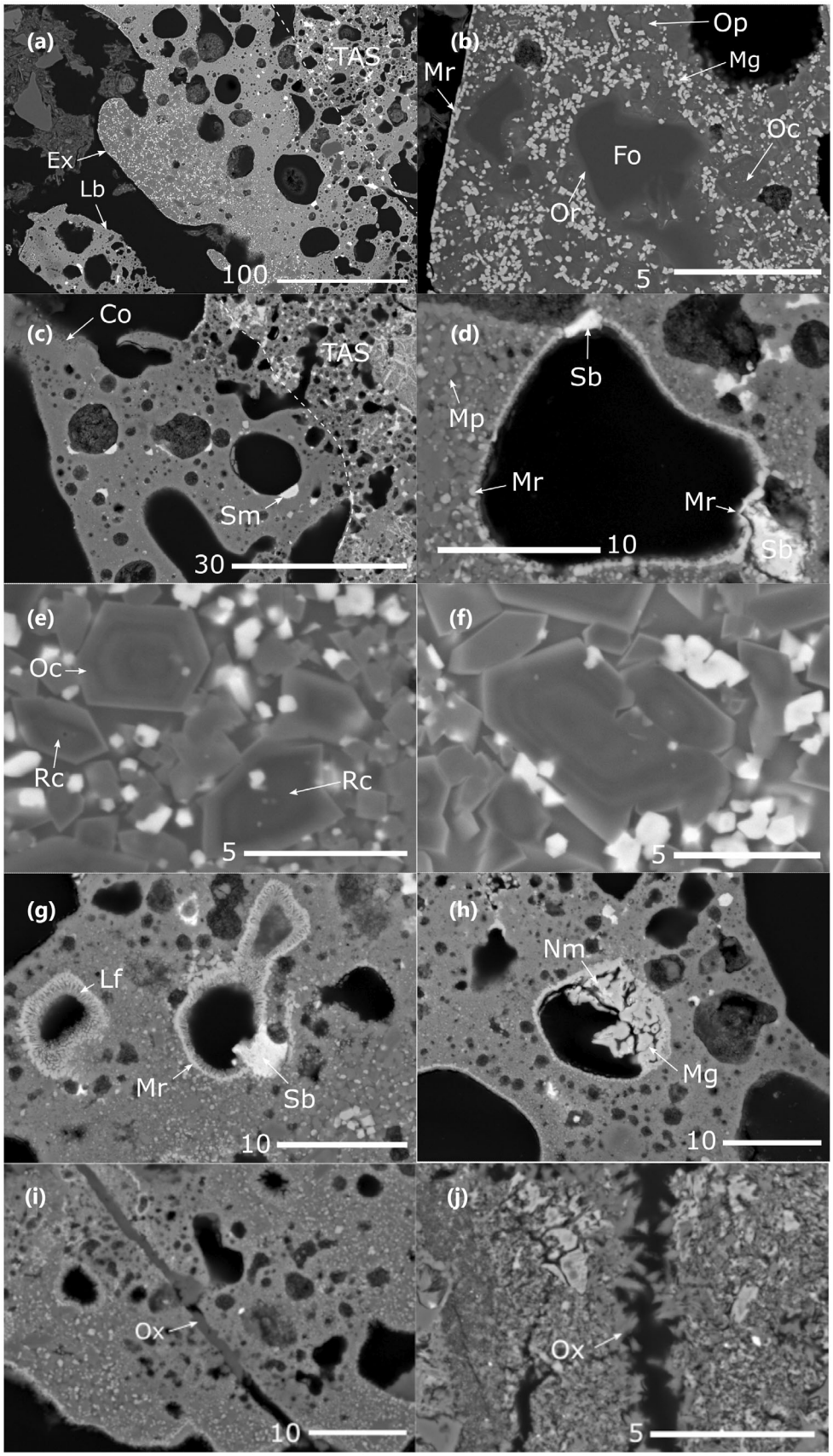

Fig. 5. Melted outer crust of Winchcombe. a) Increase in crystal size from the thermally altered substrate (TAS) to the external surface of the melted crust (TAS). Outward a lobe is also present (Lb) and is anomalous since it has a texture similar to the inner melted crust. b) Magnetite-rich (Mg) lithology containing relict forsterite (Fo) with Fe-bearing olivine rims (Or) and iron-rich relict olivine containing oxide inclusions (Oc). The mesostasis consists of olivine phenocrysts (Op) and magnetite crystals (Mg) in a glass groundmass. A magnetite rim is present on the external surface (Mr). c) A section of the inner part of the melted crust adjacent to the thermally altered substrate (TAS). The mesostasis contains cryptocrystalline olivine crystals and abundant vesicles. Sulfides (Sm) are attached to vesicles. d) A vesicle with attached sulfide blebs (Sb) and a magnetite rim (Mr). The magnetite rim coats one of the sulfide blebs. Olivine microphenocrysts (Mp) increase in size toward the outer surface of the crust (lower right). e) Zoned olivine phenocrysts and magnetite octahedra set in glass. Some phenocrysts have irregular shaped relict cores (Rc) of iron-bearing olivine. One olivine has oscillatory zoning (Oc). f) An olivine crystal containing oscillatory zoning with four iron-rich zones. g) Magnetite rims (Mr) on the inner surface of vesicles exhibiting a linear fabric (Lf). One vesicle has an attached sulfide bleb (Sb). h) A vesicle with a magnetite rim with a thicker layer of magnetite coating one side (Mg). The magnetite contains inclusions of Ni-rich metal. i) A fracture crossing the melted crust partly infilled by calcium oxalate (Ox). j) Drusy layers of oxalate crystals on a fracture in the thermal substrate. Samples are P30551—a–f, j; P30555—g–i. All scale bars are in microns.

a glassy matrix containing particularly abundant magnetite (~40 vol%) (Fig. 5b). In some less abundant areas in zoned olivine crystals were observed (Fig. 5e and 5f). Spot analyses suggest the compositions of Fa_{18}-Fa_{45}; however, the range of compositions is likely to be larger owing to the small scale of zones. Nickel contents are 0.7–1.8 wt%, but may be affected by matrix overlap with nearby magnetite. Often the crystals have an iron-bearing core, surrounded by a more magnesium-rich zone, and an outermost zone with the highest backscattered electron potential—likely to be the most fayalitic composition. Several crystals with more complex zoning patterns were observed, one with three Mg-rich zones with intervening Fe-bearing layers. These crystals can be described as having oscillatory zoning (Fig. 5e and 5f). Areas with zoned olivines tend to have low magnetite abundances (<15 vol%). Olivines sometimes contain small inclusions of iron oxides, particularly within their cores.

Relict phases are dominated by forsterite (<Fa_4) and rare enstatite (<Fs_4) and are identified by their irregular shapes and larger size than phenocrysts (Fig. 5b). They often have overgrowth rims of iron-rich olivine (Fa_{12-18}). Some relict chromite crystals are also present in the melted crust and appear as irregular, but rounded, crystals up to 15 μm in size. Often chromites are decorated by rims of equant magnetite.

Vesicles are common within the melted crust and vary between subspherical cavities and rounded elongate voids. Some extend nearly the entire thickness of the melted crust with their largest dimensions predominantly perpendicular to the melted crust–substrate boundary. Magnetite coats the surface of ~50% of vesicles (i.e., magnetite is more abundant than in the surrounding mesostasis). Magnetite occurs in rims as octahedral crystals; however, in some areas, crystals have a tabular appearance with long axes parallel to the surface (Fig. 5d). In those areas where the inner surface of the vesicle is exposed, magnetite forms elongate ridge-like features <1 μm in width (Fig. 5g). Magnetite abundance also varies around some vesicles—often forming a meniscus containing Ni-rich metal inclusions (Fig. 5h). A rim of magnetite also partially covers the external surface of the melted crust and is texturally indistinguishable from the rims on vesicles. Data from EBSD reveal that tabular magnetite crystals in the external rim define a local planar habit with [1,1,1] oriented perpendicular to the surface (Fig. 6). No stoichometric analyses of magnetite could be obtained owing to their small crystal size; however, the Ni-abundances in spot analyses suggest they contain 10–65 wt% Ni—assuming the surrounding silicates are Ni-free.

Iron–nickel sulfides are present throughout the melted crust. The majority of sulfides occur as menisci up to 5 μm in size attached to the surface of vesicles. Most vesicles with attached sulfides tend to lack magnetite rims; however, some menisci consist of a mixture of sulfide, magnetite, and Ni-rich metal (Fig. 5c). The Ni content of sulfide menisci varies from 37 to 68 wt% Ni. Metal inclusions were too small for reliable analysis; however, compositions suggest that the metal has a higher Ni content than the surrounding sulfide. Rounded blebs of Ni-bearing sulfide are also present in the mesostasis but are less abundant than menisci.

Finally, several fractures were observed cutting the melted crust and are open to the surface. Some of these features contain Ca-rich phases, some are calcite, while others have lower analytical totals (Fig. 5i). The low total phases are beam sensitive and are thus suggested to be Ca oxalates (CaC_2O_4). They are also present within some of the cracks within the thermally altered substrate and in places exhibit a drusy texture (Fig. 5j).

Magnetite Monolayers Within the Outer Melted Crust

Magnetite is distributed throughout the melted crust, most commonly as octahedra within the glassy groundmass, or as rims on some vesicles. In several locations, unusual linear trails of magnetite crystals were observed in the mesostasis as a single monolayer of magnetite crystals (Fig. 7). Analysis by EBSD of the monolayers

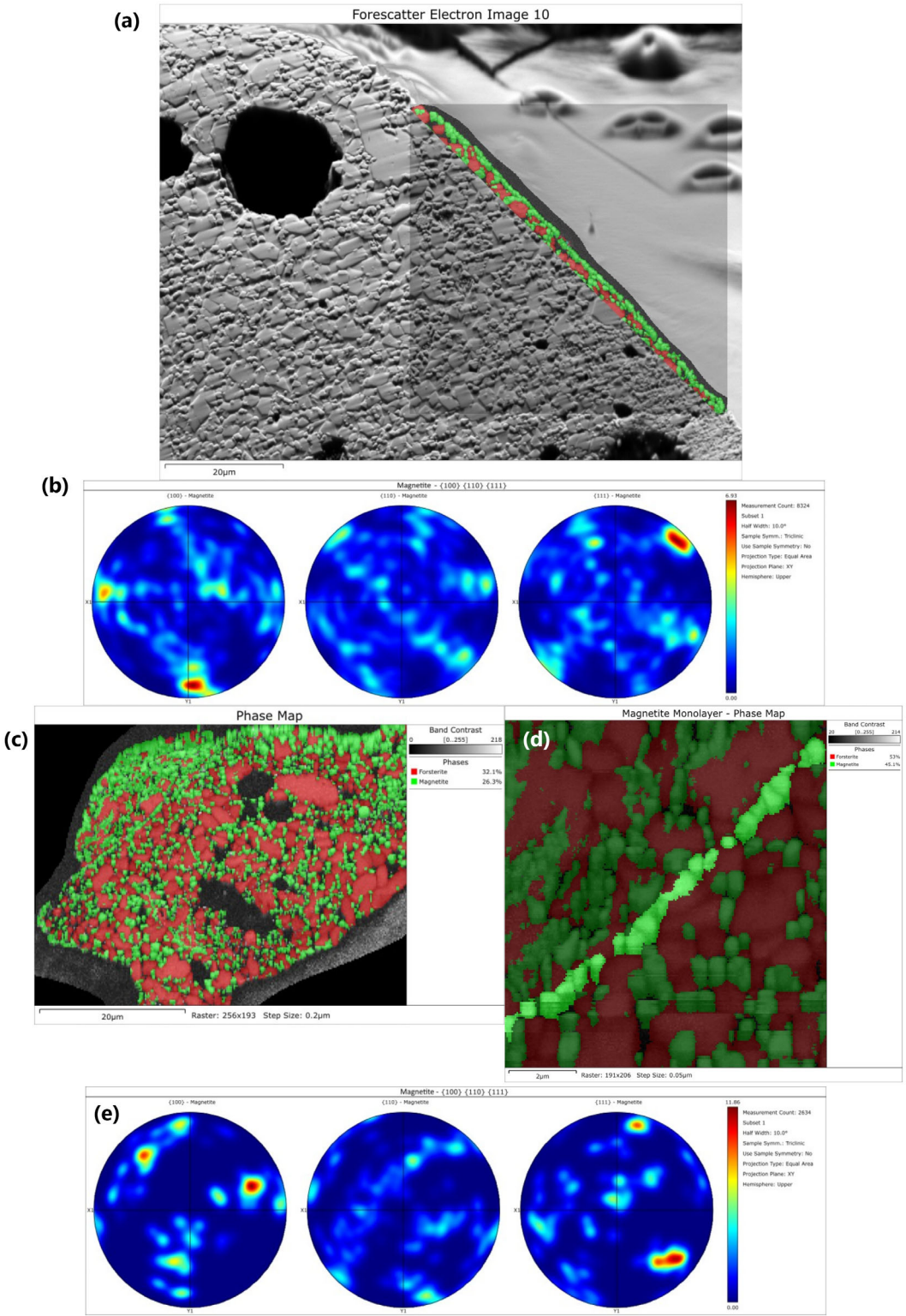

Fig. 6. EBSD data and a phase maps of tabular magnetites in the fusion crust (Block P30555). a) Forescatter electron map with a superimposed phase map of the analyzed area of the external magnetite rim (magnetite is green). b) EBSD patterns for the external magnetite rim shown in (a) showing a <111> preferred orientation. c) A phase map of wart b (olivine is red). d) Magnified phase map area shown in (c) with analyzed magnetites highlighted. e) EBSD patterns for the magnetite monolayer showing a <111> preferred orientation.

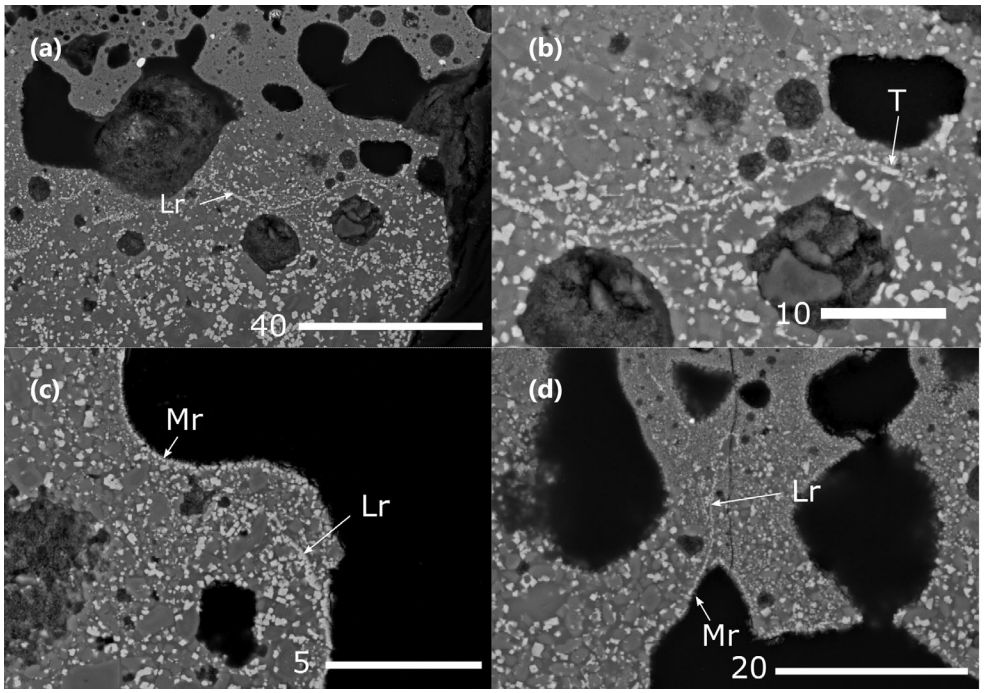

Fig. 7. Images of magnetite monolayers within fusion crust. a) A monolayer (Lr) subparallel to the melted crust–substrate boundary. b) A higher magnification image showing the presence of tabular magnetite crystals in the monolayer (T). c) A monolayer (Lr) close to the external surface of the crust that extends laterally into a magnetite rim (Mr). d) A monolayer (Lr) perpendicular to the melted crust–substrate boundary. It extends laterally into a magnetite rim (Mr). Scale bars are in microns. Images (a), (b), and (d) show sample P30555; (c) shows P30551.

indicated the magnetite crystals are oriented with [111] parallel to layering (Fig. 6).

Monolayers of magnetite were observed in P30555 and P30551 and are oriented mainly subparallel to the melted crust–substrate boundary (Fig. 7a and 7b). In one area in P30555, however, a monolayer is nearly perpendicular to the boundary and extends along its length into a magnetite rim on the external surface of the crust (Fig. 7d). Whilst in P30551 the magnetite rim on part of the surface is observed to bifurcate with one chain extending into the mesostasis (Fig. 7c).

Silicate Warts in the Outer Melted Crust

Three unusual areas of mesostasis are observed in P30555 that have different textures to other parts of the melted crust (Fig. 8). All three areas are dominated by dendritic olivine, in contrast to the euhedral olivine of the rest of the mesostases. In two of the three areas, the olivine crystals are decorated with submicron iron oxides.

One of the unusual areas of mesostasis is present as a wart-like protrusion 40 μm in length, located on the surface of the fusion crust (Fig. 8b). A magnetite monolayer separates the protrusion from the rest of the melted rim. The wart-like object also has a bimodal texture, with most of it dominated by coarse olivine dendrites (~1.5 μm in width), and an outermost part, lenticular in shape, containing fine olivine dendrites (<0.1 μm in width) and magnetite dendrites.

A second texturally distinct area is located where the surface of the crust changes orientation (Fig. 8c). This area has relatively fine olivine dendrites (<1 μm width) and contains little iron oxide.

The third distinct area is located within a subspherical region inside melted crust and contains poorly defined dendrites with abundant magnetite crystals and vesicles (Fig. 8d). A distinct magnetite rim marks the boundary with surrounding mesostasis on one side of this island-like object, while the other has a gradational boundary with the surrounding mesostasis.

Compositions

Melted Outer Crust

Compositions of the melted outer crust are shown in Table 1 and in Fig. 9 for the inner, mid, and outer parts of the crust, defined here on the basis of phenocryst size. The inner crust has olivine crystals <1 μm, the mid crust 1–4 μm, and the outer crust >4 μm. The compositions of the three silicate warts (Fig. 8) are also shown together with the bulk composition of Winchcombe as given by King et al. (2022).

The composition of the melted crust and warts has similar Ca/Si, Al/Si, Fe/Si, and Mg/Si to the bulk

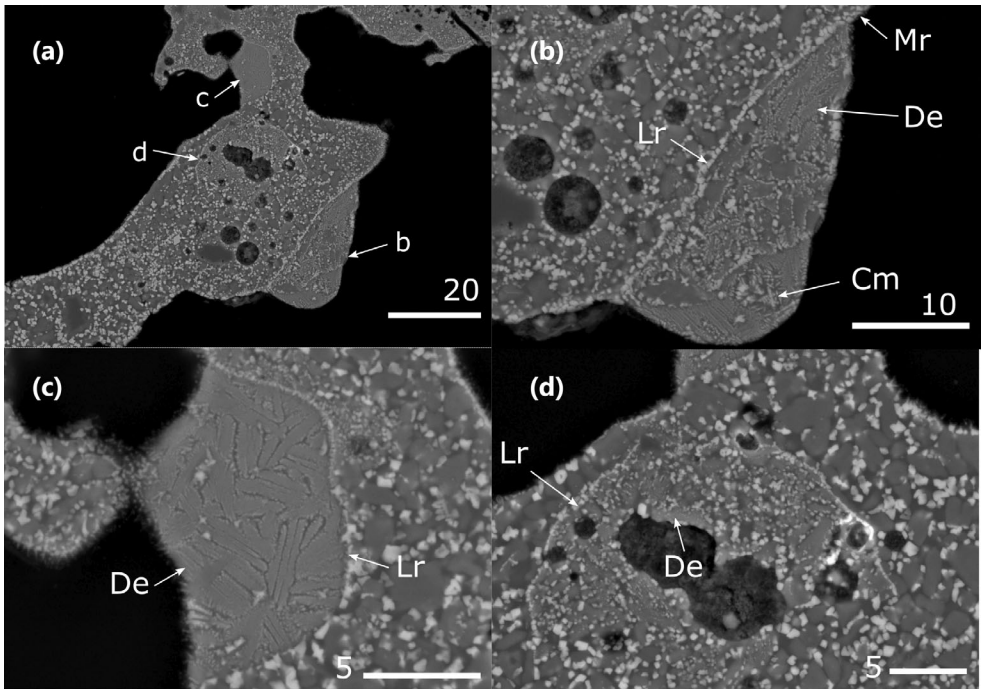

Fig. 8. Silicate warts in the outer melted crust of P30555. a) Three areas with anomalous texture located on an elongate lobe within the melted crust. b) A lenticular pimples-like body dominated by olivine dendrites (De) decorated by magnetite. The object is separated from the melted crust mesostasis by a monolayer of magnetite (Lr) that extends laterally into a magnetite rim. One area of the object has a different texture featuring smaller dendritic olivines and cruciform magnetite crystals. c) An area with olivine dendrites (De) separated from the melted crust mesostasis by a partial monolayer (Lr) of magnetite. d) An area containing poorly developed olivine dendrites (De) with abundant magnetite inclusions. A magnetite monolayer (Lr) partially surrounds the area. Downward is away from the meteorite in all images. Scale bars are in microns.

meteorite as determined by rastered area EDS analyses. Systematic variation in Mg/Si and Fe/Si is observed spatially with the inner part of the fusion crust having lower Mg/Si and higher Fe/Si, than either the mid or outer parts of the melted crust. There is no significant difference in these elements between the mid or outer parts of the melted crust. The three warts have compositions within the range of the inner/mid crust, with objects b and c having compositions within uncertainty of each other, and object d having a composition within uncertainty of the bulk meteorite.

The Ca/Si and Al/Si of most areas of the melted crust are within uncertainty of the bulk meteorite for the mid and outer crust, and warts b and c. The inner melted crust has varying Al/Si and Ca/Si with all but one enriched in Al compared to bulk meteorite. Retention of polishing material (corundum) in the small vesicles in the inner crust, however, means this could relate to contamination. Silicate wart d also has a higher Al content than bulk meteorite, and likewise has small vesicles.

The sodium abundance within the melted crust is above detection in most areas of the crust and is within uncertainty of the bulk meteorite Na/Si (0.07–0.03), albeit with some scatter to higher values. The silicate warts, however, have higher Na/Si than the mesostasis of the melted crust (>0.065). The limited range of Na/Si ratios within individual warts gives confidence that uncertainties are sufficiently small that the higher Na/Si in warts is reliable. Sulfur contents in the silicate portions of the fusion crust were below EDS detection limits. Analyses were performed on areas without sulfides.

Micro-XRF and SEM–energy dispersive X-ray maps of sample P30542 were used to derive average point and map compositions for the interior and outer melted crust and are similar to EDS rastered area analyses (Table 2). Micro-XRF maps (Fig. 10) reveal that the thermally altered substrate, as well as the outer fusion crust, is depleted in S with the interior containing 2.78 wt% while the thermally altered substrate has 1.97 wt%. Sulfur is below the micro-XRF detection limit of about 10 μg g^{-1} in the outer melted crust.

The micro-XRF map in Fig. 10d shows that the outer melted crust is enriched in Al. The abundance of Al (1.81 wt%) in the outer melted crust is compatible with the SEM-EDS values reported here (1.2–2.4 wt%), but exceeds the average value of about 0.91–0.93 wt% in the interior matrix. The concentration of Al within vesicles in the crust and in the porous outer portions of the thermally altered substrate may indicate retention of corundum polishing powder.

Table 1. Compositions of areas within the melted crust including warts b, c, and d.

	Na	Mg	Al	Si	Ca	Cr	Mn	Fe	Ni	O	Total
b	1.1	15.1	1.4	16.6	1.6	0.4	0.2	24.5	1.5	39.1	101.4
b	0.9	15.5	1.3	15.5	1.3	0.4	b.d.	24.9	1.5	37.8	99.2
b	1.2	14.7	1.5	16.1	1.6	0.3	b.d.	25.0	1.3	39.2	100.9
b	1.1	14.9	1.4	16.2	1.5	0.3	b.d.	24.3	1.4	38.4	99.5
b	1.2	14.3	1.4	16.1	1.6	0.2	0.2	25.2	1.4	38.5	100.0
c	0.9	14.1	1.4	15.6	1.3	0.3	0.3	25.0	1.4	36.6	96.9
c	0.8	13.9	1.4	15.4	1.3	0.4	0.2	24.8	1.5	36.2	95.9
d	0.9	12.8	1.8	15.6	1.5	0.4	0.3	26.6	1.6	36.5	98.2
d	1.0	12.7	1.8	15.7	1.6	0.3	0.2	26.7	1.7	36.4	98.1
Inner	b.d.	11.5	1.9	16.1	1.5	0.4	0.2	29.3	0.7	35.6	97.6
Inner	0.6	10.9	2.1	17.0	1.3	0.3	0.3	28.6	0.5	36.0	97.8
Inner	0.9	1b.d.	2.4	17.2	1.6	0.4	0.3	28.3	0.6	36.3	98.2
Inner	b.d.	11.0	2.0	16.6	1.9	0.2	0.2	28.8	0.7	35.8	97.1
Inner	0.6	14.4	1.6	16.3	1.7	0.4	0.3	25.7	1.5	36.7	99.1
Inner	0.5	14.7	1.5	16.3	1.5	0.4	b.d.	25.9	1.6	36.5	98.8
Inner	b.d.	12.9	1.7	17.1	3.7	0.2	0.2	26.1	0.3	37.4	99.7
Mid	b.d.	13.6	1.7	16.7	1.2	0.3	0.2	27.5	0.7	36.7	98.6
Mid	b.d.	13.1	1.7	16.0	2.1	0.4	b.d.	27.4	1.1	36.1	97.8
Mid	0.9	16.8	1.3	16.4	1.5	0.4	0.2	22.6	1.5	38.7	100.3
Mid	0.9	16.0	1.4	16.8	1.5	0.3	b.d.	24.3	1.4	38.0	100.5
Mid	b.d.	16.7	1.2	16.1	1.5	0.4	0.3	22.0	1.4	38.6	98.2
Mid	0.6	16.0	1.3	16.3	1.4	0.4	b.d.	24.9	1.5	37.1	99.3
Outer	0.6	15.9	1.5	17.0	1.5	0.5	b.d.	25.0	1.2	38.7	101.8
Outer	0.4	16.9	1.3	16.6	1.4	0.5	b.d.	24.1	1.4	37.8	100.5
Outer	0.7	15.2	1.4	16.0	1.5	0.4	0.2	25.5	1.5	37.5	99.9
Bulk	0.42	10.91	1.19	13.60	0.51	—	0.16	22.17	1.21	34.58	85.60

Data are in wt% and were determined by EDS. Bulk composition of the meteorite from King et al. (2022) for sample (1a-v2-1).
b.d. = below detection.

Micro-XRF maps show a small enrichment in Mg from the interior to the outer fusion crust from 11 to 14 wt%.

Sulfide Compositions

Sulfide compositions vary with depth into the meteorite and by occurrence as shown in Fig. 11. Nickel content within sulfides is highest close to the external surface of the meteorite, reaching up to 81 wt% Ni, and is lowest in the thermally altered substrate, where Ni contents are as low as 12 wt%. Sulfide blebs on the surface contain the highest overall Ni contents, while menisci contain lower average values (20–68 wt% Ni). Sulfides located in veins within the thermally altered substrate contain lower Ni contents than those in the unaltered core of the meteorite.

The sulfur contents of sulfides also vary with occurrence and location. Sulfides in the unaltered core of the meteorite are pentlandite, with (Fe + Ni)/S of 1.125, while veins in the thermally altered substrate have values of 0.95–1.18, suggesting they consist of mixtures of troilite and pentlandite. Isolated blebs of sulfide and those attached to vesicles have (Fe + Ni)/S mostly between 1.125 and 1.5, suggesting mixtures of pentlandite and heazlewoodite ($(Ni,Fe)_9S_8$). Sulfides on the surface have the lowest sulfur contents with (Fe + Ni)/S as high as 1.8. High backscattered potential phases within many of these objects are thus likely to be Ni-rich metal.

DISCUSSION

Comparison with Other Fusion Crusts

The texture of the melted fusion crust of Winchcombe is broadly similar to that of other chondritic meteorites since it consists of euhedral olivine phenocrysts set within a glassy groundmass containing magnetite octahedra (Genge & Grady, 1999a; Pittarello et al., 2019; Ramsdohr, 1967). In detail, however, the fusion crust texture most closely resembles those of CI, CM2, CR2 chondrites, since these commonly exhibit a well-defined increase in magnetite from a near magnetite-free interior region in the melted crust to a magnetite-rich outer rim (Genge & Grady, 1999a). Ordinary chondrites, in contrast, often have more abundant magnetite within the inner parts of their melted crust (Genge & Grady, 1999a).

Genge and Grady (1999a, 1999b) suggest that magnetite content is controlled principally by oxidation state during cooling. Oxidation state in meteorite fusion

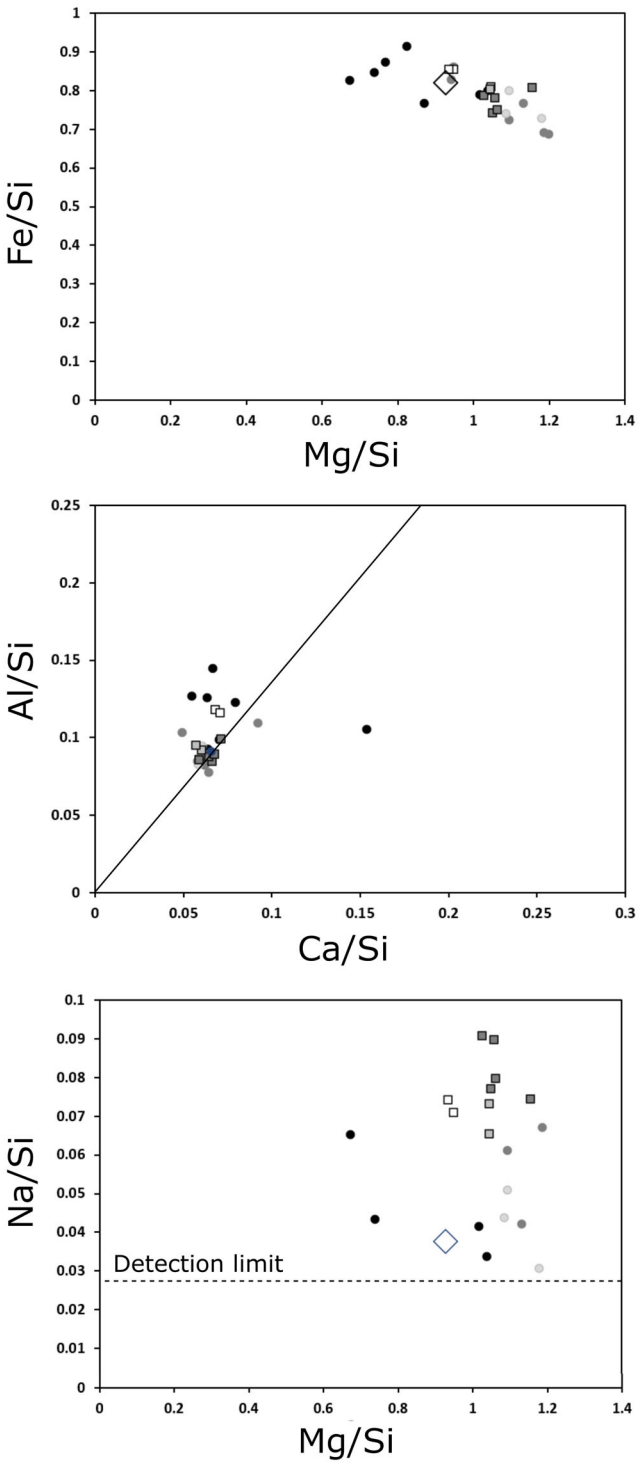

Fig. 9. Compositions of fusion crust of P30555 determined by area EDS analyses as atomic ratios. Symbols: outer melted crust—solid light gray circles, mid melted crust—medium gray circles, inner melted crust—solid black circles, silicate wart b—mid gray squares, silicate wart c—light gray squares, silicate wart d—white squares, bulk composition (King et al., 2022)—diamond.

crust is a function of mixing and implantation of atmospheric oxygen, which will vary according to altitude, and redox reactions occurring within the fusion crust. Given that cooling occurs during dark flight, which is predominantly at low altitudes of <35 km, there is likely to be only a minor control on oxidation state by altitude. Robin et al. (1992) suggested that the higher Ni contents of magnetite within meteorite fusion crusts compared with cosmic spherules relate to their deceleration at lower altitudes. The difference in terminal altitudes between meteorites may be less important than localized controls on Ni content in the fusion crust, such as the extrusion of Ni-rich sulfides through veins (Genge & Grady, 1999a).

Buffering of oxidation state by redox reactions in the thermal substrate may have a more significant effect than variations in atmospheric gas composition. Oxidative decomposition of carbonaceous materials and sulfides are sinks for oxygen that cause reduction and are observed within the fusion crusts of CI, CM2, CR2 (Genge & Grady, 1999a); enstatite chondrites (Genge & Grady, 1999b); and ureilites (Pittarello et al., 2019). Localized variations in oxidation state in fusion crusts have previously been suggested to occur in the vicinity of large metal grains within ordinary chondrite fusion crusts (Genge & Grady, 1999a). In the Winchcombe crust, the occurrence of magnetite-rich areas with relatively Mg-rich olivines, and magnetite-poor regions with zoned Fe-bearing olivines, likewise implies spatial variations in oxidation state. Differences in the local abundance of sulfide might lead to such variations since their oxidative degassing may act as a sink for oxygen.

The increase in olivine crystal size through the Winchcombe fusion crust is similar to other stony meteorites. The occurrence of large numbers of small crystals close to the substrate and large euhedral crystals near the put surface is probably the result of the destruction of crystallization nuclei with increasing temperature toward the exterior. Large crystals grow where lower densities of crystal nuclei compete for components in the melt. Crystals grow during cooling of the melt layer as heating subsides on deceleration.

The composition of the fusion crust of Winchcombe exhibits a similar evolution to other chondritic fusion crusts with no major depletions in moderate volatiles, such as Na, compared with the bulk meteorite. This behavior contrasts with the significant depletion of Na from cosmic spherules owing to their larger surface area to mass ratios (Genge et al., 2018). Nevertheless, cooling rate and time spent at high temperature are also crucial in Na-loss, as illustrated by the detectable Na found in airburst debris particles (Van Ginneken et al., 2010, 2012, 2021).

Table 2. Bulk composition of slice P30542 and average compositions of melted outer crust and thermally altered substrate (micro-XRF data) compared against SEM-EDS averages of the interior of slice P30542 and average Winchcombe fusion crust.

	Interior			Outer melted crust	Thermally altered substrate	
	Map[a]	Point[a] $n = 113$	Point[b]	Point[a] $n = 20$	Point[a] $n = 15$	Average fusion crust Point[b]
wt%						
Na	0.34	0.35	0.18	0.38	0.36	0.3–0.9
Mg	11.01	11.58	11	14.02	12.46	b.d.
Al	0.91	0.93	1.22	1.81	1.00	1.2–2.4
Si	10.72	11.24	13.1	12.71	12.15	16–17
P	0.04	0.04	b.d.	0.04	0.03	b.d.
S	2.78	3.03	2.41	b.d.	1.97	b.d.
K	0.01	0.01	0.03	0.01	0.02	b.d.
Ca	0.86	1.00	0.14	0.99	0.25	1.3–2.1
Ti	0.07	0.07	0.05	0.05	0.06	b.d.
Cr	0.29	0.29	0.21	0.30	0.29	0.2–0.4
Mn	0.18	0.19	0.22	0.18	0.21	0.2–0.3
Fe	20.07	21.37	25.9	19.31	23.53	22–27
Ni	1.11	1.18	1.54	1.18	1.23	0.3–1.5
$\mu g\ g^{-1}$						
V	15	12	b.d.	54	41	b.d.
Co	1297	1327	b.d.	377	469	b.d.
Cu	212	160	b.d.	158	171	b.d.
Zn	222	130	b.d.	146	120	b.d.
Total	47.45	50.26	56	49.87	52.43	—

n denotes the number of individual point analyses averaged; b.d. = below detection.
[a]Micro-XRF data.
[b]SEM-EDS data.

No systematic search for lateral variations in fusion crust composition was performed in this study; however, the extrusion mechanisms that cause lateral changes by localized magma mixing, proposed by Genge and Grady (1999a), are unlikely to occur in the absence of chondrules with glassy mesostases or large grains of metal or sulfides. These variations are pronounced in ordinary chondrites. Like in most meteorites, the Fe/Si, Mg/Fe, and Ca/Si ratios in Winchcombe fusion crust are thus very similar to those of the bulk meteorite.

The observed subtle variation in chemistry through the fusion crust, with a more Mg-rich, Fe-poor outermost layer, could be produced during or after deceleration. Iron exchange between immiscible sulfide liquids and the silicate melt of the melted crust provides one viable explanation, since Fe-enriched crusts have been previously observed adjacent to large metal grains in fusion crusts (Genge & Grady, 1999a). In Winchcombe, the large abundance of newly formed sulfide at the melted crust–substrate might provide a mechanism for this Fe enrichment, by exchange of Fe between sulfide droplets and the surrounding silicate melt. Indeed, the observation that sulfides become progressively Ni-rich testifies that this exchange occurs. This mechanism, however, can only explain the compositional variation through the melted crust if it occurs during cooling since otherwise Fe loss from the silicate melt is required during the production of the outer layers of the melted crust by progressive heating of the underlying melt. Iron loss by evaporation can probably be discounted, owing to the lack of Na depletions, even though experimental studies of fusion crust formation indicate Fe evaporation does occur earlier in flight (Helber et al., 2019). Furthermore, the interaction of immiscible sulfides with the silicate melt causes Fe enrichment, rather than depletion, in this oxidizing environment.

An alternative explanation for the variation in Fe/Mg through the melted crust is provided by the progressive melting of relict Mg silicates from the melted crust–substrate boundary to the surface. Melting of Mg-rich relict silicates will operate while heating is ongoing (i.e., during deceleration) and would necessarily imply that mixing of melt is insufficient to entirely remove compositional differences. An interesting implication of such a mechanism is that ablation particles removed from surface melt layers are unlikely to have compositions

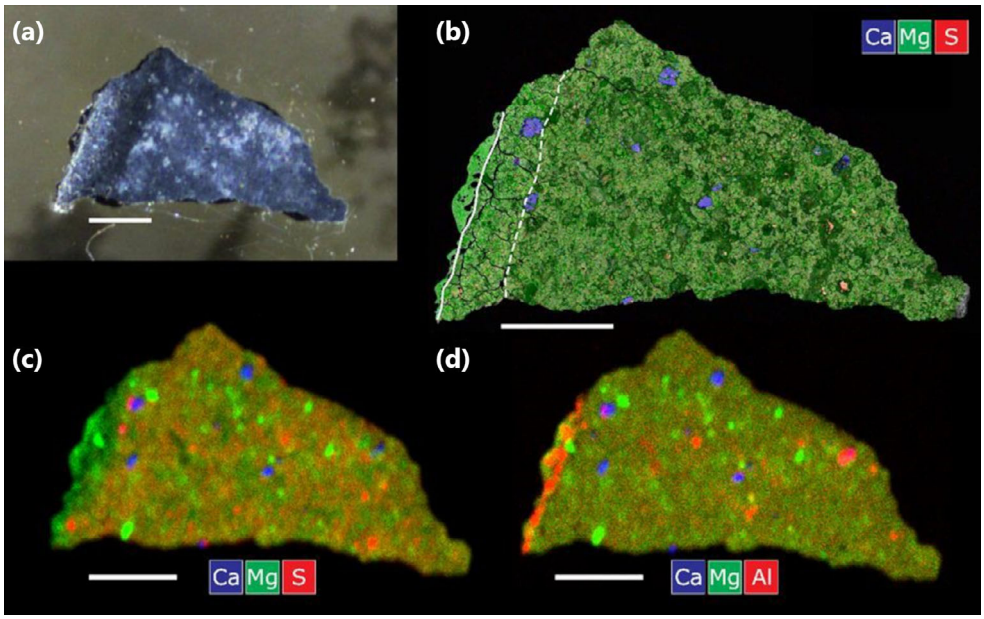

Fig. 10. Slice P30542 (the scale bar in each panel is 1 mm). a) Optical image in reflected light. b) SEM-EDS element distribution map of Ca (blue), Mg (green), and S (red). The solid white line marks the boundary of the melted outer crust; the dashed line marks the approximate boundary of the thermally altered substrate (cf. Fig. 2). c) Micro-XRF element distribution map of Ca (blue), Mg (green), and S (red). d) Micro-XRF element distribution map of Ca (blue), Mg (green), and Al (red). Note that the thermally altered substrate is more heavily fractured than the bulk of the sample. From (c) and (d), the fusion crust can be seen to be depleted in S and enriched in Al.

identical to the bulk meteorite, and might have spatially variable compositions, if they sample different parts of the melt layer.

Fracture Networks

The presence of fracture networks in the thermally altered substrates of carbonaceous chondrites has previously been noted by Genge and Grady (1999a) and suggested to be the result of contraction of matrix during dehydration. The development of these dehydration cracks is, therefore, a function of the degree of contraction of the matrix, and thus sensitive to matrix mineralogy. Winchcombe exhibits higher volumes of dehydration cracks than observed in other carbonaceous chondrites, including the CI chondrites Orgueil and Alais (Genge & Grady, 1999a). The degree of contraction of matrix on dehydration is not, however, a simple factor of phyllosilicate content. Amorphous phyllosilicate gels, for example, may undergo more contraction during hydration owing to their adsorbed water than crystalline clay minerals. Tochilinite also undergoes contraction and has a lower decomposition temperature than serpentine—the dominant phyllosilicate (Fuchs et al., 1973). The occurrence of such abundant dehydration cracks associated with the dominant tochilinite-rich lithology of Winchcombe, and not other lithologies, suggests that its mineralogical assemblage is more prone to contraction.

Dehydration cracks have previously been suggested to promote the fragmentation of hydrous micrometeorites during their atmospheric entry heating (Genge, 2008; Suttle et al., 2019). In meteorites, they are likely to play a similar role, albeit one restricted to the removal of the outermost layers to a depth comprising a significant thickness of the thermal substrate. Removal of this layer, at least at a late stage in deceleration, is suggested by the observation that fusion crust is present as small, isolated areas on some of the Winchcombe stones (Fig. 1a)—a feature similar to many other CM2 and CI chondrites.

Some evidence for the rapid loss of surface layers might explain an interesting feature of the Winchcombe fireball, observed in video footage. After an initial flare, the fireball is seen to produce multiple small pulses of plasma, with a semi-periodic duration of ~200 ms (Fig. 12a). These pulses are clearly not associated with large-scale fragmentation events of the bolide since no separation is observed (cf. Peekskill fireball). Instead, the plasma traverses along the trail until it fades after ~0.5 s. Periodic loss of the surface layer of the meteorite might explain such a pulsed increase in ionized material, with a time scale related to heat transfer and dehydration of the thermal substrate. Although a possible explanation for these observations, pulsed, semi-periodic changes in luminosity in fireballs has been observed instrumentally and is explained by coupled hydrodynamic–thermal

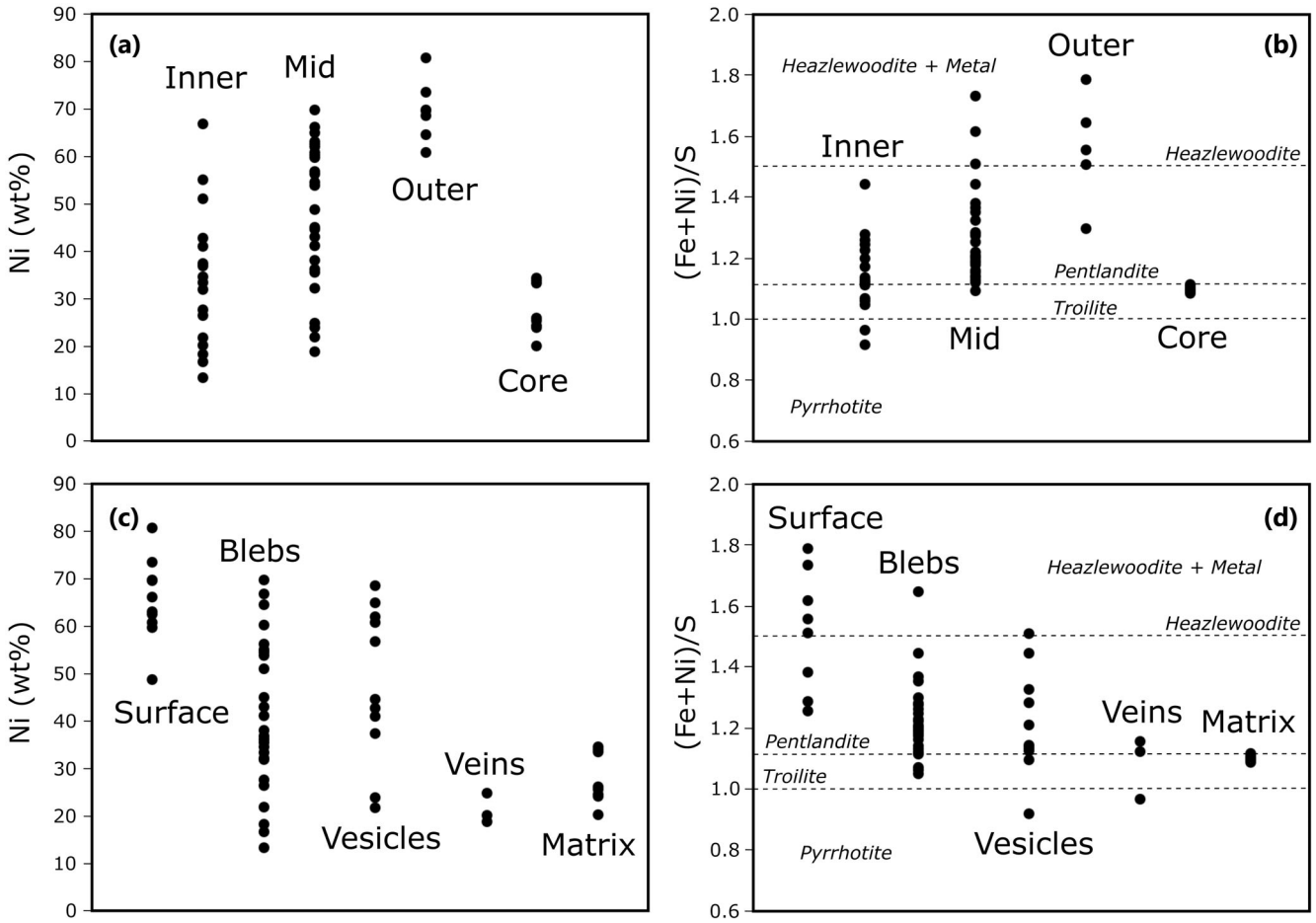

Fig. 11. Compositions of Fe-Ni-sulfides in the fusion crust by position (a, b) and by occurrence (c, d). Sulfides marked as matrix were measured in the interior below the inner margin of the thermally altered substrate. The inner, mid, and outer melted crust are shown. Veins were present within the thermally altered substrate. Blebs were mainly present in the inner melted crust and the outermost part of the thermally altered substrate.

instability (heating–melting–blow away–vaporization cycle of the meteoroid surface; Borovička et al., 2015) or rotation (Spurný et al., 2012) and occur on similar time scales. Unusually, for the Winchcombe fireball, however, these variations were observable with the naked eye. If large-scale loss of surface layers is responsible, however, such calving events may inject large numbers of particles, with size distributions dictated by the crack network, into the trail gas stream. Interestingly, Winchcombe was associated with a persistent smoke trail supporting significant loss of small particulates. The trail also shows variations in particle density along its length, although these could also relate to varying dispersion rates rather than initial particle number density (Fig. 12b).

Finally, dehydration of phyllosilicates is strongly endothermic, providing an additional heat sink. This effect is observed during the atmospheric entry of hydrated micrometeorites, which despite their small size, develop large thermal gradients supported by the endothermic thermal decomposition of phyllosilicates (Genge, 2006; Genge, Suttle, et al., 2017; Suttle et al., 2017). The thermal gradient into hydrated carbonaceous chondrites is thus likely to be greater than ordinary chondrites or achondrites, albeit complicated by variations in heating related to preferred flight orientation of faces (Sears, 1975).

Zoning of Olivine Phenocrysts and Thermal History

Zoning of olivine phenocrysts has previously been described in meteorite fusion crusts (Genge & Grady, 1999a; Pittarello et al., 2019) and within S-type cosmic spherules (Genge et al., 2018). Pittarello et al. (2019) have previously reported reverse and oscillatory zoned olivine phenocrysts within ordinary chondrite and ureilite fusion crusts; however, most of these grains had iron-rich cores and rims with intervening Mg-rich layers. Such crystals could form by the overgrowth of olivine on relict Fe-bearing olivine cores as described for both fusion crusts

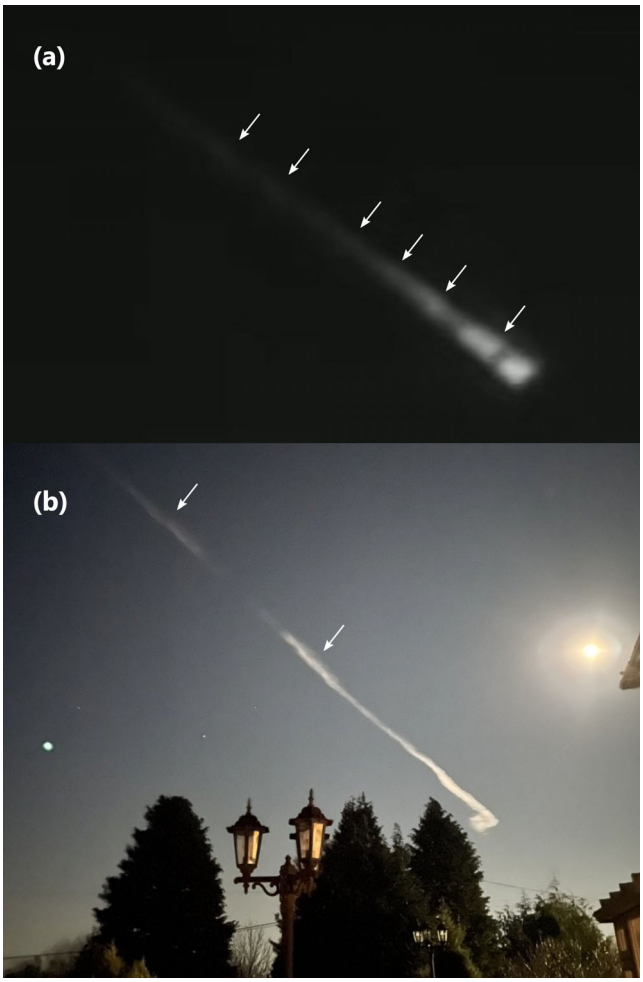

Fig. 12. Images of the Winchcombe fireball and trail. a) A frame from studio security camera footage over Midsomer Norton, UK of the Winchcombe fireball. Bright pulses of plasma within the trail are labeled by arrows. b) A photograph of the persistent trail illuminated by the full moon, as seen from Ruardean Hill, Gloucestershire. © Daniel M. (imo.net).

(Genge & Grady, 1999a) and cosmic spherules (Genge et al., 2018). Some olivine crystals with multiple repeating zones were also described by Pittarello et al. (2019), but were skeletal and thus complicated by the penetration of melt into crystals. Oscillatory zoning in terrestrial skeletal olivine is known to be subject to out of sequence growth (Salas et al., 2021), but this cannot apply to the euhedral crystals in Winchcombe fusion crust.

Typically, oscillatory zoning within igneous rocks forms owing to an instability driven by competition between growth rate and diffusion (Allègre et al., 1981). Elements with low diffusion rates within the melt and crystal are more likely to exhibit oscillatory zones. In olivine, oscillatory zones have, for example, been observed in P, in crystals having Fe-Mg normal zones owing to the slow diffusion of P compared to Fe and Mg (Milman-Barris et al., 2008). Unusually, rapid olivine growth in fusion crust would be required to form Fe-Mg oscillatory zones by diffusive instability, but is not consistent with the euhedral crystal shapes present. Furthermore, arguably more extreme thermal behavior is experienced by S-type cosmic spherules which do not exhibit oscillatory zoning in Fe-Mg within olivine.

Oxygen fugacity variations have previously been suggested to cause oscillatory zoning in fusion crust (Pittarello et al., 2019), although as described above, these zoning profiles are likely not to be oscillatory sensu stricto, instead being iron-bearing relict cores or nonsequential dendritic growth. Changes in Fe^{3+}/Fe^{2+} in the melt could plausibly cause zoning, and there is certainly evidence for spatial variation in fO_2 in the melted crust of Winchcombe on scales comparable to melted crust width. The preservation of fine oscillatory zones, however, necessitates fO_2 fluctuations over very short periods that are unlikely to be consistent with the time scales imposed by diffusion of oxygen within melt. Consequently, temperature fluctuations seem a more likely explanation for the presence of oscillatory zoning in fusion crust.

The origin of temperature fluctuations in the surface melt layer on bolides could arise simply through hydrodynamic instability leading to pressure changes in the bow shock and fluctuating adiabatic heating of gas (Krinov, 1960). Heat transfer to the melt layer occurs rapidly by thermal radiation from the hot bow shock. Rotation of a meteoroid could also lead to periodic temperature fluctuations through changing illumination by the radiative heat flux. Both hydrodynamic instability and rotation, however, fail to explain the rarity of oscillatory zoned olivine in fusion crust, since both of these processes are common, if not ubiquitous, in fireballs. Conversely, the removal of significant proportions of the surface layer into the gas stream, as suggested above, might have a similar effect owing to the additional radiative flux liberated by gas drag heating of the released particles. Oscillatory zoning in olivines in fusion crust might, therefore, record the thermal history during the late stages of deceleration. Since they are rarely observed, they suggest Winchcombe's thermal behavior was somewhat different to most meteorites, as does its large abundance of dehydration cracks.

Sulfide Generation and Behavior in Fusion Crusts

There is a general increase in sulfide abundance with decreasing depth in the thermal substrate of the Winchcombe meteorite, with a maximum immediately below the melted crust. The occurrence of sulfide also changes through the fusion crust with pre-existing grains and thin veins within cracks present in most of the substrate, to dispersed blebs and sulfide-lined or filled

veins in the shallow substrate, and finally menisci and blebs in the outer fusion crust. An increasing spatial association of sulfide with magnetite and Ni-rich metal is observed toward the exterior of the meteorite.

The generation of sulfide in the fusion crust of Winchcombe is most likely to occur owing to the thermal decomposition of tochilinite. The dominant lithologies contain abundant TCIs (B1/B2; Daly et al., this volume; King et al., 2022; Suttle et al. this volume), while they contain only sparse sulfide grains, dominated by pentlandite. Too little sulfide exists in the interior of Winchcombe to produce the sulfide within the fusion crust. Furthermore, textural evidence for thermal decomposition of tochilinite is observed, with the appearance of cavities and loss of sheet-like habits, consistent with its low-temperature stability (<250 °C; Fuchs et al., 1973). The observation that sulfide veins first appear within TCIs and then become more abundant toward the fusion crust as TCIs become increasingly altered is evidence that tochilinite is the dominant source of sulfide liquid.

The occurrence of sulfides within small areas of fractures within the thermal substrate is consistent with their migration within fractures. As low viscosity liquids, eutectic sulfide melts are readily capable of flow in thin veins. Outward flow is suggested by the increasing abundance of sulfide outward culminating in the highest abundance at the outermost parts of the thermal substrate. Direct evidence for this process, by which eutectic sulfide melts are focused into fractures, and then migrate outward, has been observed in experimental heating studies of ordinary chondrites with real-time observation of sulfide liquids by computed tomography scanning (Panerai et al., 2021). However, the driving force for outward migration is problematic since capillary forces, which affect liquids flowing within cracks, will cause inward migration owing to the inward tapering of dehydration cracks in the thermal substrate. Thermal expansion of melts, combined with the increase in volume on melting, may well provide some of the impetus for migration, but is inconsistent with the occurrence of sulfides as coatings or over short segments of a crack. A likely alternative is the migration of sulfide liquids through gas production and expansion during devolatilization of the thermal substrate. Water vapor will be generated by the dehydration of phyllosilicates, while SO_2 is produced by oxidative decomposition of sulfides. Expansion of these gases will force eutectic sulfide liquids through the crack network.

An interesting implication of gas mediated fluid flow through the dehydration crack network is its role in heat transfer. Suttle et al. (2019) discussed the role of devolatilization in heat transport in micrometeorites and illustrated the inward heat transport and increased thermal alteration in the vicinity of dehydration cracks. Micrometeorites, however, are small objects in which surface melt seals the interior. Fusion crusts are tabular on the length scales of gas escape and the presence of cavities penetrating through the melted outer crust to the substrate imply melt removal by gas loss, implying high internal gas pressures. Indeed, gas pressure may also assist the fragmentation of the surface layer of meteorites containing abundant dehydration cracks, such as CI and CM2 chondrites.

Within the outer melted crust, sulfides are present as menisci and blebs. These are evidently immiscible sulfide liquids within the silicate melt of the mesostasis. The location of the majority of sulfides as menisci on vesicles suggests gas migration is also important in their transport within the outer crust. Surface tension effects, driven by the low contact angles of sulfide liquids on silicates (Gaetani & Grove, 1999), will strongly attach sulfide menisci to vesicles and spread them around the boundary of the cavity. Sulfide liquids will, therefore, be transported outward on vesicles and be brought toward the surface of the crust, providing a mechanism by which they can be separated. Consequently, meteorites in addition to cosmic spherules (Genge & Grady, 1998) might also produce Fe-Ni metallic droplets.

The low contact angles of sulfide liquids on silicate melts have previously been noted by Taylor et al. (2011) on S-type cosmic spherules and explain how sulfide melts migrate across their surfaces. In cosmic spherules, the sulfides undergo oxidative thermal decomposition on the surface of particles where they are exposed to atmospheric gas, to form magnetite. In outer melted crusts, the formation of films of sulfide along the surfaces of vesicles might likewise be affected by oxidative loss of SO_2 producing a residue of magnetite. The occurrence of magnetite rims lining some vesicles in Winchcombe is consistent with this model, with at least one example (Fig. 5h) preserving the original meniscus morphology.

Oxidation of sulfides explains the increase in Ni content of these phases outward since the transformation of iron to the divalent state allows its partitioning into the surrounding silicates while Ni is retained by the residual liquid. The decrease in sulfur content is likewise compatible with oxidative decomposition to produce SO_2. In the melted crust, magnetite rims are observed only on some vesicles, but not on others, and on the external surface of the melt layer, suggesting that access of atmospheric gas is an important factor. Magnetite-lined vesicles, thus, may be open to the surface out of the plane of section. Vesicles with sulfide menisci without magnetite rims, in contrast, may be sealed and cannot be accessed by the atmosphere. Ultimately complete oxidation of sulfides leads to magnetite formation; however, the high initial Ni content of the sulfide requires

the observed exsolution of Ni-rich metal from the produced oxides. This process also occurs within I-type cosmic spherules where oxidation leads to the production of progressively smaller residual Ni-rich metal beads and exsolution of Ni-rich metal from magnetite (Brownlee et al., 1983; Genge, Davies, et al., 2017).

Magnetite Monolayers

The observation of chains of magnetite crystals within the Winchcombe melted crust has not been previously reported in meteorite fusion crusts. These internal monolayers of magnetite extend from the external surface into the mesostasis, suggesting they are related to surface magnetite rims, which are likewise monolayers. A genetic link is also supported by the presence of tabular crystals in magnetite rims, contrary to their usual octahedral habits and face-centered (inverse spinel) cubic crystal lattices that tend to lead to equant crystal forms. Crystal habits, however, are also influenced by growth factors. In the case of magnetite rims, the proximity of the free surface leads to a lower diffusive supply of components in this direction and preferential growth parallel to the surface. The observation of linear ridges of magnetite on the surface of the outer crust might also suggest that flow may play a role in moderating diffusive supply. The best developed face [111] aligns to the liquid interface by surface tension leading to the preferred orientation seen in both the external rims and the magnetite monolayers (Fig. 6). The presence of tabular magnetite crystals in monolayers inside the mesostasis, together with their preferred [111] orientations, strongly suggests that these originally grew within a magnetite rim located at the melt–atmosphere interface.

A plausible mechanism to explain how magnetite monolayers grow on the surface and then become incorporated in the mesostasis is provided by the irregular geometry of the fusion crust melt layer. The melt layer has highly variable thickness and exhibits numerous lobe-like protrusions. It is likely that these geometries are produced by vigorous gas loss through the melted crust—the gas forcing pathways and perhaps removing melt. This scenario would be highly dynamic over short periods, in particular when combined with atmospheric gas flow across the surface of the meteorite. Indeed, surface striations observed on the surface of the Winchcombe fusion crust (Fig. 1) testify to lateral flow of melt across the surface. Collapse of melt protrusions back onto the surface is thus highly likely to have occurred and would be expected to envelop the existing melt interface trapping any magnetite rim that had previously formed. The collapse of vesicles through gas lost through open channels to the surface may also have a similar effect and helps explain how magnetite chains could form perpendicular, as well as quasi-parallel, to the melt–substrate surface. The rarity of such features in fusion crusts implies that Winchcombe's volatile loss was unusually vigorous, perhaps owing to a combination of volatile content, sensitivity of mineralogy to dehydration, and the large abundance of gas loss pathways in the form of dehydration cracks.

Silicate Warts and Intershower Melt Transfer

Warts of silicate melt having textures different from the rest of the melted crust are highly unusual and have not been previously reported in studies. The presence of monolayers of magnetite separating warts from the rest of the melted crust implies these surfaces formed at the melt–atmosphere interface. An unavoidable interpretation, therefore, is that warts were liquid droplets that impacted the surface. Areas with texture such as Fig. 8d could, in contrast, represent melts that penetrated along pathways into the melt layer since the surface is topographically complex. Indeed, the partially gradational boundary on one side of the observed island is consistent with mixing into the melt of the outer crust.

Transfer of liquid droplets onto the outer melted crust is consistent with the fluid dynamical environment of bolides. Oriented stones, for example, commonly exhibit numerous protrusions on the backward facing surface formed by the collision of droplets drawn into this low-pressure region from the gas stream (Krinov, 1960). Pittarello et al. (2019) also reported a spherical glassy object on the surface of the fusion crust of an ordinary chondrite, which could be a droplet formed by ablation. An interesting question is, however, whether these attached droplets were the result of transfer from one area to another on the same stone, or between stones of the same shower.

Given that stones in the same shower have approximately the same bulk composition, it is unlikely their ablation droplets will be chemically distinct. In the case of the three objects reported here, all have Mg/Si, Fe/Si, and Ca/Si within uncertainty of the bulk meteorite composition. Similar compositional homogeneity was suggested by Harvey et al. (1998) and Van Ginneken et al. (2021) as a signature of ablation debris.

The textures of the three objects show a significant difference to those of the mesostasis of the melted crust since they exhibit dendritic crystals. The presence of dendrites implies higher peak temperatures, owing to the destruction of crystallization nuclei. Contrary to expectation, however, the Na/Si ratios of the objects are higher than the melted crust mesostasis, suggesting they have not experienced more evaporation. In general, however, the Na content of fusion crusts is not

significantly depleted compared with bulk meteorite composition (Genge & Grady, 1999a). Variations in alkali metal contents within fusion crusts, for example, in areas generated on different lithologies, are entirely possible leading to small differences between stones.

One scenario that could produce higher temperature liquid droplets is their production on the surface of a separate stone in the shower, which was traveling at a slightly higher velocity. Although consistent with the observation that the fragmentation of Winchcombe did occur to produce separate stones separated across the strewn field, video footage does not record major fragmentation and separation of fragments at least during luminous flight that would be consistent with significantly different velocities of nearby fragments. An alternative at lower relative velocities might be additional heating of droplets by gas drag after they had been removed from another stone into the gas stream, although high Na partial pressures within the gas stream would be required to prevent significant additional evaporative loss of Na from small droplets. The observed silicate warts are good candidates for the first intershower transfer particles recorded in fusion crust. Their rarity also implies extreme behavior, consistent with vigorous gas loss or dehydration mediated calving to produce unusually abundant particulates—although serendipitous transfer, owing to a close pass of two shower members cannot be excluded.

A puzzling property of the warts is the wide variation in magnetite abundance. Warts d and b contain approximately the same abundance of magnetite as the fusion crust mesostasis and yet wart c is almost magnetite free. Given the Mg/Si and Fe/Si ratios of the three warts are all similar, different oxygen fugacities are likely to be responsible for the variation in magnetite abundance, suggesting wart c experienced lower fO_2 than the other objects. Since these were droplets released into the gas stream, it is unexpected that one object would have a lower fO_2 than either the fusion crust mesostasis or other droplets. However, incomplete equilibration with atmosphere, perhaps owing to residence time in the gas stream, could explain differences between droplets, and would be consistent with release from different stones in the shower. It does not explain, however, why the fO_2 of one droplet was lower than the fusion crust mesostasis.

Variations in fO_2 in the outer fusion crust between stones of Winchcombe are not recorded in any of the samples, which all have similar textures and mineralogies. Localized reduction in outer melted crust, however, can occur in proximity to reducing agents such as metal or carbonaceous material (Genge & Grady, 1999a). Reduction in an area of fusion crust that produced wart c might, therefore, be plausibly caused by proximity to a concentration of C- and N-rich globules observed in the meteorite (King et al., 2022). Alternatively, fO_2 also varies in the gas stream as a consequence of gas pressure, which varies significantly between the front and rear faces of stones, with net fO_2 also influenced by rotation. The production of wart c from a rear face might thus also result in a lower fO_2. Finally, the fO_2 in the outer melted crust is seen to increase from the substrate–melted crust interface to the external surface. Production of wart c from the innermost melt layer could, therefore, explain its lower fO_2, but would necessarily require additional heating in the gas stream to remove crystallization nuclei to produce the observed dendritic structure.

Weathering

Calcium-oxalate was observed in sections P30551, P30554, and P30555. Open fractures to the surface partially in-filled with Ca-oxalate suggest very rapid weathering of CM2 chondrites can occur in temperate environments. Ca-oxalate is likely to form by the hydrous dissolution of a highly soluble Ca-rich components within the meteorite. Although calcite is present within the interior, the unusual occurrence of oldhamite (Daly et al., 2022, this volume) may be significant since it is sensitive to dissolution.

Similar to the Ca-oxalate, Jenkins et al. (this volume) observed Ca-rich phases occurring in large fractures within the thermally altered substrate of the section P30552. The Ca-rich phases occurred in veins about tens of microns thick and gave Raman spectra being consistent with calcite, the majority of which was poorly crystalline. Like the Ca-oxalate, it also formed from rapid weathering, where Ca-rich components were dissolved and precipitated as calcite.

The samples which contain terrestrial oxalate and carbonates were recovered on farmland near Rushbury House on March 6, and although no precipitation was reported over this period, the English countryside in February is not known for its arid nature, and dew and fog did occur. This is not the first fall to show the growth of terrestrial evaporate phases, as terrestrial carbonates were found growing in a sample of the CV chondrite Vigarano that spent a month outdoors after its fall (Abreu & Brearley, 2005) and terrestrial sulfates are known to occur in Ivuna (King et al., 2022). Jenkins et al. (this volume) also found terrestrial sulfates occurring in areas outside the fusion crust within the P30552 section of Winchcombe. Other studies have shown early weathering occurs in meteorites (e.g., Van Ginneken et al., 2022); however, these observations emphasize that terrestrial alteration occurs rapidly and that even meteorites observed to fall are not exempt. It also suggests that fusion crust provides an opportunity to demonstrate the terrestrial origins of alteration products.

IMPLICATIONS

Observations on the fusion crust of Winchcombe reveal that several previously unknown processes occur during atmospheric flight. Interestingly, the most unusual features of Winchcombe fusion crust, namely the large abundance of dehydration cracks, are likely to have indigenous origins related to material properties of the meteoroid, rather than its entry parameters. The mineralogy and composition of its matrix are evidently highly susceptible to contraction of dehydration of clay minerals and tochilinite compared to most other carbonaceous chondrites. The unique nature of the matrix of the dominant TCI-rich lithology in Winchcombe is also supported by its unusual textural features (Daly et al., this volume; King et al., 2022; Suttle et al., this volume).

The unusual dehydration behavior of Winchcombe may also have caused observable phenomena, as well as being recorded in the petrology of the fusion crust. The presence of oscillatory zoning within olivine phenocrysts is potentially the result of significant temperature variations during flight and is consistent with observations of quasi-periodic plasma production by the bolide. A model in which these fluctuations are caused by periodic loss of fusion crust, owing to mechanical weakening by intense fracturing, also agrees with the observation of liquid droplets potentially derived by transfer between stones in the same shower. This is mostly likely where particle production is high, for example, when delamination of the fractured thermal substrate occurs.

Observations of intense periodic changes in luminosity of bolides might provide indications that the mineralogy of meteoroids is particularly sensitive to dehydration with resulting production of particles by calving. However, mechanisms that likewise produce light curve periodicity, such as rotation (Spurný et al., 2012) and instabilities (Borovička et al., 2015), complicate the interpretation of bolides. It does, however, provide a mechanism by which the mineralogical properties of the meteoroid can affect its optical behavior during deceleration.

The Winchcombe fusion crust also has interesting implications for the microscopic ablation debris that is produced by the atmospheric entry of meteorites. Although the global mass of this debris is likely to be significantly smaller than cosmic dust, owing to the smaller total mass of the meteorite flux, it could be locally abundant enough to be detected in surface deposits and provide a proxy for meteorite falls that have not been recovered. Indeed, some more energetic bolides that undergo terminal detonations do generate large quantities of dust-sized debris in the form of airburst particles. It is unlikely, however, that any of those meteoroids survived to reach the Earth's surface (Badyukov et al., 2011; Badyukov & Raitala, 2012; Harvey et al., 1998; Van Ginneken et al., 2010, 2012, 2021).

The observation that intense dehydration of some CM2 chondrites produces an intersecting network of dehydration cracks may make them produce larger quantities of ablation debris than other chondrites. The characteristic size of fragments observed here suggests these particles are rarely larger than 70 μm in diameter, and become more abundant with smaller size. Additional size decrease owing to evaporation during gas drag heating after release is also possible. Silicate warts observed in Winchcombe indeed testify to the higher temperatures experienced by ablation materials by continued heating, although the lack of depletions in Na suggests little additional evaporation. Winchcombe, however, is anomalous compared to most CM2 chondrites owing to its low entry velocity of 13.5 km s^{-1} (compared to 28 km s^{-1} for Sutter's Mill and Maribo; Borovička et al., 2019; Jenniskens et al., 2012), and it is thus possible that Na contents of ablation spherules vary with entry velocity providing a proxy for their atmospheric behavior.

It is highly likely that ablation debris will have complex size distributions since it can be produced by several discrete processes. Debris generated by fragmentation events will depend on the mechanical properties or the interior, with size distributions that are influenced by preatmospheric weakness, such as the fractures and intraclast matrix observed in Winchcombe (Daly et al., this volume; Suttle et al., this volume). Calving of substrates by dehydration cracks will have length scales that relate to the degree of contraction on dehydration, and thus on phyllosilicate content and mineralogy.

Removal of melt droplets from the surface of the outer melted crust is a likely mechanism to produce ablation debris. The size distribution of these particulates will be influenced by factors that control the thickness of the layer. Previous studies of meteorite fusion crust have described thickness variations owing to lateral flow, with accumulation of melt on the reverse face of oriented stones (Ramsdohr, 1967), and the formation of thin secondary crusts by the delamination of areas of pre-existing crust. On Winchcombe, lateral flow is recorded by longitudinal and lateral flow ridges on some faces, with accumulation of melt evident in the significant differences in melted crust thickness. Lateral flow ridges show the movement of melt en masse probably owing to ripple-like instabilities resulting in melting collecting in the gas flow. These are probably features of stages of deceleration where slip flow dominates over the surface rather than a stagnant boundary layer. Explosive gas release from the interior may also influence the size of ablation droplets produced from the outer melted crust given the observation of large vesicles truncating melted crust and lobe-like protrusions in Winchcombe. If lobes were removed by this process, then gas release could

generate some droplets several hundred microns in diameter.

Most of the mechanisms of ablation debris production are sensitive to the material properties of the meteoroid, as well as the hydrodynamic behavior. Mechanical fragmentation is related to tensile strength and pre-existing structural weaknesses. Gas loss-mediated production of ablation debris will be related to the abundance, distribution, and mineralogy of volatile-bearing phases (phyllosilicates, sulfides, and carbonates). Ablation debris produced by different types of meteorite may, therefore, vary not only in composition but also in size distribution.

Some features observed in the Winchcombe meteorite crust might provide an indicator for ablation materials produced by vigorous gas loss. Magnetite monolayers within the melted crust are likely to be the result of disturbance of the surface layer by vigorous gas loss as a consequence of intense dehydration. These suggest that fusion crusts record more complex histories than previously supposed, recording multiple events that occurred in the last few seconds of high-temperature flight. These events are also likely to be preserved within ablation debris.

Finally, Winchcombe testifies to the complexity of chemical fractionation within fusion crust, despite its small thickness. Eutectic sulfide liquids can evolve through a complex reaction pathway including decomposition of mineral phases and reaction in the presence of reductive agents. Migration and concentration of eutectic liquids toward the base of the melted outer crusts occur in Winchcombe and are facilitated by dehydrations cracks. Then, migration through the melted crust occurs by surface tension interactions with vesicles commensurate with oxidative enrichments in nickel. This process of extreme enrichment of Ni through loss of S and exchange of iron with the silicate melt leads to the production of submicron grains of Ni-dominated metal which has interesting implications for the bioavailability of this element considering their large surface area to volume ratios.

CONCLUSIONS

The petrology and mineralogy of the fusion crust of Winchcombe broadly resemble other stony meteorites, and in particular CM2 chondrites. Several features were, however, recognized that have not been previously reported and reveal processes occurring during atmospheric entry. Unusually abundant dehydration cracks observed in the thermally altered substrate of the Winchcombe meteorite testify to the high abundance of phyllosilicate and its mineralogy indicating it is particularly susceptible to contraction on heating. This weakened layer is highly likely to undergo failure during deceleration and inject debris into the meteoroid trail, leading to heating and plasma generation—phenomena evident in video observations of the Winchcombe fireball. Oscillatory zoning observed within olivine phenocrysts in the fusion crust is rare in other meteorites, and could also be related to episodic mass loss events during deceleration as a result of temperature fluctuations. Other unusual features in Winchcombe may relate to the volatile-rich nature of the meteoroid since they testify to explosive gas loss during heating. Magnetite monolayers observed within the fusion crust have not previously been described and most likely formed by the collapse of protrusions of melt trapping magnetite rims formed on the surface of the melt layer. The formation of such protrusions is likely to be driven by explosive loss of gas through the molten crust. Finally, several areas with dendritic textures, different from the rest of the melted crust were observed, which are consistent with the re-accretion of molten ablation debris. Their dendritic textures imply higher peak temperatures and are consistent with debris transferred between stones of the same shower, which undergo additional heating in the gas stream. These represent the first discovery of intra-shower transfer of ablation materials.

Acknowledgments—This publication is part of the Winchcombe science team consortium, organized by the UK Fireball Alliance, and conducted by the UK Cosmochemistry Network. The authors of this paper would like to thank the UK Fireball Alliance, its constituent networks (UK Fireball Network, SCAMP, UKMON, AllSky7, NE MATODE, GMN), international collaborators (FRIPON, Global Fireball Observatory, Desert Fireball Network, University of Western Ontario, and University of Helsinki), and the meteor observation camera owners who participate in the UK Fireball Alliance network for their aid in observing the fireball and helping to predict its fall position. We would also like to thank the scientists and volunteers who participated in the UK Fireball Alliance–led search and recovery of the Winchcombe meteorite, and the local community, who generously reported and donated meteorite finds and enabled the team to search the strewn field. STFC are acknowledged for supporting the "Curation and Preliminary Examination of the Winchcombe Carbonaceous Chondrite Fall" project (ST/V000799/1), and Natural History Museum staff for curatorial support.

Data Availability Statement—The data that support the findings of this study are provided in tables and images in the results section of the paper.

Editorial Handling—Dr. Donald E. Brownlee

REFERENCES

Abreu, N. M., and Brearley, A. J. 2005. Carbonates in Vigarano: Terrestrial, Preterrestrial, or Both? *Meteoritics & Planetary Science* 40: 609–25.

Allègre, C., Provost, A., and Jaupart, C. 1981. Oscillatory Zoning: A Pathological Case of Crystal Growth. *Nature* 294: 223–8.

Artemieva, N. A., and Shuvalov, V. V. 2016. From Tunguska to Chelyabinsk Via Jupiter. *Annual Review of Earth and Planetary Sciences* 44: 37–56.

Badyukov, D. D., Ivanov, A. V., Raitala, J., and Khisina, N. R. 2011. Spherules from the Tunguska Event Site: Could They Originate from the Tunguska Cosmic Body? *Geochemistry International* 49: 641–53.

Badyukov, D. D., and Raitala, J. 2012. Ablation Spherules in the Sikhote Alin Meteorite and Their Genesis. *Petrology* 20: 520–8.

Borovička, J., Popova, O., and Spurný, P. 2019. The Maribo CM2 meteorite fall - survival of weak material at high entry speed. *MAPS* 54: 1024–1041.

Borovička, J., Spurný, P., Šegon, D., Andreić, Ž., Kac, J., Korlević, K., Atanackov, J., et al. 2015. The Instrumentally Recorded Fall of the Križevci Meteorite, Croatia, February 4, 2011. *Meteoritics & Planetary Science* 50: 1244–59.

Brownlee, D. E., Bates, B., and Beauchamp, R. H. 1983. Meteor Ablation Spherules as Chondrule Analogs. In *Chondrules and Their Origins*, edited by A. King, 10–25. Houston, Texas: Lunar and Planetary Institute.

Campbell-Burns, P., and Kacerek, R. 2014. The UK Meteor Observation Network. *WGN, Journal of the International Meteor Organization* 42: 139–44.

Colas, F., Zanda, B., Vernazza, P., Vaubaillon, J., Bouley, S., Gattaccecca, J., Baratoux, D., et al. 2012. (FRIPON) Fireball Recovery and Interplanetary Matter Observation Network. *Asteroids, Comets, Meteors*, 1, abstract 6426.

Court, R. W., and Sephton, M. A. 2009. Meteorite Ablation Products and Their Contribution to the Atmospheres of Terrestrial Planets: An Experimental Study Using Pyrolysis-FTIR. *Geochimica Cosmochimica Acta* 73: 3512–21.

Daly, L., McMullan, S., Rowe, J., Collins, G. S., Suttle, M., Chan, Q. H. S., Young, J. S., et al. 2020. The UK Fireball Alliance (UKFAll): Combining and Integrating the Diversity of UK Camera Networks to Aim to Recover the First UK Meteorite Fall for 30 Years, Europlanet Science Congress 2020, Online, 21 September–9 October 2020, EPSC2020-705.

Devillepoix, H. A. R., Cupák, M., Bland, P. A., Sansom, E. K., Towner, M. C., Howie, R. M., Hartig, B. A. D., et al. 2020. A Global Fireball Observatory. *Planetary and Space Science* 191: 105036.

Fuchs, L. H., Olsen, E., and Jensen, K. J. 1973. Mineralogy, Mineral-Chemistry, and Composition of the Murchison (C2) Meteorite. *Smithsonian Contributions to the Earth Sciences* 10: 1–39.

Gaetani, G. A., and Grove, T. L. 1999. Wetting of Mantle Olivine by Sulfide Melt: Implications for Re/Os Ratios in Mantle Peridotite and Late-Stage Core Formation. *Earth and Planetary Science Letters* 169: 147–63.

Genge, M. J. 2006. Igneous Rims on Micrometeorites. *Geochimica et Cosmochimica Acta* 70: 2603–21.

Genge, M. J. 2008. Micrometeorites and Their Implications for Meteors. *Earth Moon and Planets* 102: 525–35.

Genge, M. J., Davies, B., Suttle, M., Van Ginneken, M., and Tomkins, A. 2017. The Mineralogy and Petrology of I-Type Cosmic Spherules: Implications for Their Sources, Origins and Identification in Sedimentary Rocks. *Geochimica et Cosmochimica Acta* 218: 167–200.

Genge, M. J., and Grady, M. M. 1998. Melted Micrometeorites from Antarctic Ice with Evidence for the Separation of Fe-Ni-S Liquids During Entry Heating. *Meteoritics & Planetary Science* 33: 425–34.

Genge, M. J., and Grady, M. M. 1999a. The Fusion Crusts of Stony Meteorites: Implications for the Atmospheric Reprocessing of Extraterrestrial Materials. *Meteoritics & Planetary Science* 34: 341–56.

Genge, M. J., and Grady, M. M. 1999b. Unequilibrated Assemblages of Sulphide, Metal and Oxide in the Fusion Crusts of the Enstatite Chondrite Meteorites. *Mineralogical Magazine* 63: 473–88.

Genge, M. J., Suttle, M., and Van Ginneken, M. 2017. Thermal Shock Fragmentation of Mg Silicates Within Scoriaceous Micrometeorites Reveal Hydrated Asteroidal Sources. *Geology* 45: 891–4.

Genge, M. J., Van Ginneken, M., Suttle, M., and Harvey, R. 2018. Accumulation Mechanisms of Micrometeorites in an Ancient Supra-Glacial Moraine at Larkman Nunatak, Antarctica. *Meteoritics & Planetary Science* 53: 2051–66.

Hankey, M., Perlerin, V., and Meisel, D. 2020. The All-Sky-6 and the Video Meteor Archive System of the AMS Ltd. *Planetary and Space Science* 190: 105005.

Harvey, R. P., Dunbar, N. W., McIntosh, W. C., Esser, R. P., Nishiizumi, K., Taylor, S., and Caffee, M. W. 1998. Meteoritic Event Recorded in Antarctic Ice. *Geology* 26: 607–10.

Helber, B., Dias, B., Bariselli, F., Zavalan, L. F., Pittarello, L., Goderis, S., Soens, B., McKibbin, S. J., Claeys, P., and Magin, T. E. 2019. Analysis of Meteoroid Ablation Based on Plasma Wind-Tunnel Experiments, Surface Characterization, and Numerical Simulations. *Astrophysical Journal* 876: 120.

Jenniskens, P., Fries, M. D., Yin, Q.-Z., Zolensky, M., Krot, A. N., Sandford, S. A., Sears, D., et al. 2012. Radar-Enabled Recovery of the Sutter's Mill Meteorite, a Carbonaceous Chondrite Regolith Breccia. *Science* 338: 1583–7.

King, A., Daly, L., Rowe, J., Joy, K. H., Greenwood, R. C., Devillepoix, H. A. R., Suttle, M. D., et al. 2022. The Winchcombe Meteorite, a Unique and Pristine Witness from the Outer Solar System. *Science* 8: 1–17.

Krinov, E. L. 1960. *Principles of Meteoritics*. New York: Permagon Press.

McMullan, S., Vida, D., Devillepoix, H. A. R., Rowe, J., Daly, L., King, A. J., Cupall, M., Howie, R. M., and Sansom, E. K. 2022. The Winchcombe Fireball—That Lucky Survivor.

Miller, S. D., Straka, W. C., Bachmeier, A. S., Schmit, T. J., Partain, P. T., and Noh, J.-T. 2013. Earth-Viewing Satellite Perspectives on the Chelyabinsk Meteor Event. *Proceedings of the National Academy of Sciences* 110: 18092–7.

Milman-Barris, M., Beckett, J., Baker, M., Hofmann, A., Morgan, Z., Crowley, M., Vielzeuf, D., and Stolper, E. 2008. Zoning of Phosphorus in Igneous Olivine. *Contributions to Mineralogy and Petrology* 155: 739–95.

Panerai, F., Bessire, B., Haskins, J. B., Foster, C., Barnard, H. S., Stern, E., and Feldman, J. 2021. Morphological

Evolution of Ordinary Chondrite Microstructure During Heating: Implications for Atmospheric Entry. *The Planetary Science Journal* 2: 179.

Pittarello, L., Yamaguchi, A., Roszjar, J., Debaille, V., Koeberl, C., and Claeys, P. 2019. To Be or Not to Be Oxidized: A Case Study of Olivine Behavior in the Fusion Crust of Ureilite A 09368 and H Chondrites A 09004 and A 09502. *Meteoritics & Planetary Science* 54: 1563–78.

Ramsdohr, P. 1967. Die schmelzkruste der meteorite. *Earth and Planetary Science Letters* 2: 593–8.

Robin, E., Bonte, P., Froget, L., Jehanno, C., and Roccia, R. 1992. Formation of Spinels in Cosmic Objects During Atmospheric Entry—A Clue to the Cretaceous-Tertiary Boundary Event. *Earth and Planetary Science Letters* 108: 181–90.

Salas, P., Ruprecht, P., Hernandez, L., and Rabbia, P. 2021. Out-of-Sequence Skeletal Growth Causing Oscillatory Zoning in Arc Olivines. *Nature Communications* 12: 4069.

Sears, D. W. 1975. Temperature Gradients in Meteorites Produced by Heating During Atmospheric Passage. *Modern Geology* 5: 155–64.

Spurný, P., Bland, P. A., Shrbený, L., Borovička, J., Ceplecha, Z., Singelton, A., Bevan, A. W. R., et al. 2012. The Bunburra Rockhole Meteorite Fall in SW Australia: Fireball Trajectory, Luminosity, Dynamics, Orbit, and Impact Position from Photographic and Photoelectric Records. *Meteoritics & Planetary Science* 47: 163–85.

Stewart, W., Pratt, A. R., and Entwisle, L. 2013. NEMETODE: The Network for Meteor Triangulation and Orbit Determination. System Overview and Initial Results from a UK Video Meteor Network. *WGN, Journal of the International Meteor Organisation* 41: 84–91.

Suttle, M., Genge, M., Folco, L., Van Ginneken, M., Lin, Q., Russell, S., and Najorka, S. 2019. The Atmospheric Entry of Fine-Grained Micrometeorites: The Role of Volatile Gases in Heating and Fragmentation. *Meteoritics & Planetary Science* 54: 503–20.

Suttle, M. D., Genge, M. J., Folco, L., and Russell, S. S. 2017. The Thermal Decomposition of Fine-Grained Micrometeorites, Observations from Mid-IR Spectroscopy. *Geochimica et Cosmochimica Acta* 206: 112–36.

Taylor, S., Jones, K. W., Herzog, G. F., and Hornig, C. E. 2011. Tomography: A Window on the Role of Sulfur in the Structure of Micrometeorites. *Meteoritics & Planetary Science* 46: 1498–509.

Van Ginneken, M., Debaille, V., Decrée, S., Goderis, S., Woodland, A. B., Wozniakiewicz, P., De Ceukelaire, M., Leduc, T., and Claeys, P. 2022. Artificial Weathering of an Ordinary Chondrite: Recommendations for the Curation of Antarctic Meteorites. *Meteoritics & Planetary Science* 57: 1247–66.

Van Ginneken, M., Folco, L., Perchiazzi, N., Rochette, P., and Bland, P. A. 2010. Meteoritic Ablation Debris from the Transantarctic Mountains: Evidence for a Tunguska-Like Impact over Antarctica ca. 480 ka Ago. *Earth and Planetary Science Letters* 293: 104–13.

Van Ginneken, M., Goderis, S., Artemieva, N., Debaille, V., Decree, S., Harvey, R. P., Huwig, K. A., et al. 2021. A Large Meteoritic Event over Antarctica ca. 430 ka Ago Inferred from Chondritic Spherules from the Sor Rondane Mountains. *Science Advances* 7: 2375–548.

Van Ginneken, M., Suavet, C., Cordier, C., Folco, L., Rochette, R., Sonzogni, C., and Perchiazzi, N. 2012. Oxygen Isotope Composition of Meteoritic Ablation Debris from the Transantarctic Mountains: Constraining the Parent Body and Implications for the Impact Scenario. *Meteoritics & Planetary Science* 47: 1738–47.

Vida, D., Šegon, D., Gural, P. S., Brown, P. G., McIntyre, M. J., Dijkema, T. J., Pavletić, L., et al. 2021. The Global Meteor Network—Methodology and First Results. *Monthly Notices of the Royal Astronomical Society* 506: 5046–74.